RAG suppresses group 2 innate lymphoid cells

Aaron M. Ver Heul[1], Madison Mack[2], Lydia Zamidar[3,4,5,6], Masato Tamari[3,4,5,6,], Ting-Lin Yang[8], Anna M. Trier[8], Do-Hyun Kim[9,10], Hannah Janzen-Meza[1], Steven J. Van Dyken[9], Chyi-Song Hsieh[11], Jenny M. Karo[12], Joseph C. Sun[12], Brian S. Kim[3,4,5,6,7,*]

[1]Division of Allergy and Immunology, Department of Medicine, Washington University School of Medicine, St. Louis, MO 63130, USA

[2]Immunology & Inflammation Research Therapeutic Area, Sanofi, Cambridge, MA 02141, USA

[3]Kimberly and Eric J. Waldman Department of Dermatology, Icahn School of Medicine at Mount Sinai, New York, NY 10029, USA

[4]Mark Lebwohl Center for Neuroinflammation and Sensation, Icahn School of Medicine at Mount Sinai, New York, NY 10019, USA

[5]Marc and Jennifer Lipschultz Precision Immunology Institute, Icahn School of Medicine at Mount Sinai, New York, NY 10029, USA

[6]Friedman Brain Institute, Icahn School of Medicine at Mount Sinai, New York, NY 10029, USA

[7]Allen Discovery Center for Neuroimmune Interactions, Icahn School of Medicine at Mount Sinai 10019

[8]Division of Dermatology, Department of Medicine, Washington University School of Medicine, St. Louis, MO 63130, USA

[9]Department of Pathology and Immunology, Washington University School of Medicine, St. Louis, MO 63130, USA

[10]Department of Life Science, College of Natural Sciences, Hanyang University, Seoul 04763, Republic of Korea

[11]Division of Rheumatology, Department of Medicine, Washington University School of Medicine, St. Louis, MO, USA.

[12]Immunology Program, Memorial Sloan Kettering Cancer Center, New York, NY 10065, USA; Immunology and Microbial Pathogenesis Program, Graduate School of Medical Sciences, Weill Cornell Medical College, New York, NY 10065, USA.

*Correspondence: Brian S. Kim, MD, MTR, Icahn School of Medicine at Mount Sinai, 1425 Madison Avenue, New York, NY, 10029. E-mail: brian.kim3@mountsinai.org

ABSTRACT

Antigen specificity is the central trait distinguishing adaptive from innate immune function. Assembly of antigen-specific T cell and B cell receptors occurs through V(D)J recombination mediated by the Recombinase Activating Gene endonucleases RAG1 and RAG2 (collectively called RAG). In the absence of RAG, mature T and B cells do not develop and thus RAG is critically associated with adaptive immune function. In addition to adaptive T helper 2 (Th2) cells, group 2 innate lymphoid cells (ILC2s) contribute to type 2 immune responses by producing cytokines like Interleukin-5 (IL-5) and IL-13. Although it has been reported that RAG expression modulates the function of innate natural killer (NK) cells, whether other innate immune cells such as ILC2s are affected by RAG remains unclear. We find that in RAG-deficient mice, ILC2 populations expand and produce increased IL-5 and IL-13 at steady state and contribute to increased inflammation in atopic dermatitis (AD)-like disease. Further, we show that RAG modulates ILC2 function in a cell-intrinsic manner independent of the absence or presence of adaptive T and B lymphocytes. Lastly, employing multiomic single cell analyses of RAG1 lineage-traced cells, we identify key transcriptional and epigenomic ILC2 functional programs that are suppressed by a history of RAG expression. Collectively, our data reveal a novel role for RAG in modulating innate type 2 immunity through suppression of ILC2s.

INTRODUCTION

Atopic disorders such as atopic dermatitis (AD), asthma, and food allergy are associated with T helper type 2 (Th2) cell responses, elevated production of the type 2 cytokines interleukin(IL)-4, IL-5, and IL-13, and induction of immunoglobulin(Ig)E[1–4].Classically, this allergic inflammatory cascade is believed to originate with antigenic stimulation of T cell receptors on adaptive T cells, which in turn results in the production of IgE from B and plasma cells capable of binding the same antigen. Indeed, presence of antigen-specific IgE reactivity is a hallmark across atopic disorders.[5] Thus, for decades, antigen-specific adaptive Th2 cell responses have been the primary focus of investigation in the pathogenesis of atopic diseases. However, recent studies indicate that innate immune cells are sufficient to not only drive allergic pathology, but also amplify adaptive Th2 cell responses[6–9]. These studies suggest that innate immune mechanisms may play a larger role in driving atopic inflammation than previously recognized.

Innate lymphoid cells (ILCs), while lacking antigen receptors generated by recombination activating gene proteins RAG1 and RAG2 (collectively called RAG), are the innate counterparts of T cells. For example, ILC2s mirror adaptive Th2 cells in their developmental requirements, cytokine profiles, and effector functions[10]. Unlike classical T cells, ILC2s are concentrated at barrier surfaces to rapidly respond to microbial and environmental stimuli. ILC2s are key mediators of inflammatory skin conditions like AD[11–13]. Indeed, in murine models of AD-like disease, type 2 skin inflammation can still occur despite the absence of adaptive T cells, but is further reduced after depletion of ILC2s[12,13]. Furthermore, recent studies have shown that ILC2s harbor non-redundant functions in the presence of the adaptive immune system in the setting of anti-helminth immunity[14,15]. These findings suggest that ILC2 dysfunction may also uniquely contribute to the pathogenesis of atopic diseases, independent of adaptive immunity. However, the cell-intrinsic mechanisms that drive ILC2 dysregulation remain poorly understood.

ILC2s were originally discovered due to their capacity to orchestrate multiple allergic pathologies in immunocompromised mice, most notably in RAG-deficient mice that lack T and B cells[16–22]. These discoveries fundamentally redefined our understanding of allergic diseases and placed a major focus on ILC2s as potential drivers of human allergic disease. However, despite ILC2s not requiring RAG expression for their development, fate mapping studies in mice have demonstrated that up to 60% of ILC2s have historically expressed RAG1 during development[23,24]. Although previous work has described roles of RAG beyond antigen receptor recombination in developing T and B cells[25–27] and NK cells[24], how this developmental expression of RAG impacts ILC2s remains unclear.

By directly comparing RAG-deficient and RAG-sufficient mice, we unexpectedly found enhanced AD-like disease in RAG-deficient mice, despite the lack of adaptive lymphocytes to contribute to AD-like inflammation. Using splenocyte replenishment and bone marrow chimeras, we show that RAG suppresses ILC2 activation and expansion in a cell-intrinsic manner. Employing a RAG1-lineage reporter mouse line, we performed simultaneous single-cell multiomic RNA and ATAC sequencing to show that RAG fate-mapped ILC2s display unique transcriptional and epigenomic alterations consistent with the suppression of effector cytokine production. Collectively, our studies reveal evolutionarily conserved regulatory functions of RAG within innate lymphocytes, extending beyond the generation of antigen receptors in adaptive lymphocytes.

RESULTS

RAG deficiency leads to expansion and activation of ILC2s

AD-like disease can be elicited in the skin of mice with repeated application of the topical vitamin D analog calcipotriol (MC903)[28]. Although it has been previously demonstrated that MC903 can

98 induce AD-like disease in RAG-deficient mice that lack T and B cells, in part via ILC2
99 activation[12,13], the relative contributions of ILC2s and the adaptive lymphocyte compartment have
100 not been rigorously evaluated. We hypothesized that the presence of Th2 cells, in addition to
101 ILC2s, would lead to enhanced AD-like disease in an additive fashion. In testing this, we evaluated
102 both RAG1-sufficient wild-type (WT) mice and RAG1-deficient *Rag1*$^{-/-}$ mice in the setting of AD-
103 like disease (**Fig. 1A**). Unexpectedly, we observed that *Rag1*$^{-/-}$ mice developed increased ear skin
104 thickness (**Fig. 1B**) and higher frequencies of ILC2s in the skin-draining lymph nodes (sdLNs)
105 compared to control WT mice (**Fig. 1C, S1A,B**). Furthermore, a larger proportion of ILC2s from
106 *Rag1*$^{-/-}$ mice exhibited production of both IL-5 (**Fig. 1D, S1C**) and IL-13 (**Fig. 1E, S1C**). Our
107 findings indicated that RAG1 deficiency results in paradoxically worse AD-like disease in
108 association with enhanced ILC2 expansion and activation.

109 To determine whether this phenomenon was specific to AD-like pathological conditions,
110 we next examined the sdLNs in *Rag1*$^{-/-}$ and lymphocyte-sufficient *Rag*$^{+/-}$ littermate control mice in
111 the absence of disease (**Fig. 1F**). We found that the frequency of ILC2s was increased at steady
112 state in *Rag1*$^{-/-}$ sdLNs (**Fig. 1G**) and that a higher proportion of these ILC2s produced both IL-5
113 (**Fig. 1H**) and IL-13 (**Fig. 1I**) compared to WT controls. The RAG recombinase requires both
114 RAG1 and RAG2 components to successfully rearrange a functional antigen receptor in adaptive
115 lymphocytes[29]. Thus, to test whether our findings are specific to RAG1, or related to function of
116 the overall RAG complex, we similarly examined the steady-state profile of ILC2s in *Rag2*$^{-/-}$ mice
117 (**Fig. S2A**). Deficiency of RAG2 led to an expansion of ILC2s in the sdLNs (**Fig. S2B**) and
118 increased proportions of ILC2s expressing IL-5 (**Fig. S2C**) and IL-13 (**Fig. S2D**) similar to *Rag1*$^{-/-}$
119 mice. Collectively, these findings suggest that the RAG recombinase modulates ILC2 function at
120 steady state and during type 2 inflammation. However, whether the hyperactive ILC2 phenotype
121 is due to a cell-intrinsic process or simply due to the absence of T and B cells was unclear.

122

123 **ILC2 suppression by RAG is cell intrinsic**

124 Given the importance of the adaptive lymphocyte compartment in shaping the secondary
125 lymphoid organ repertoire, we next wanted to examine whether the presence of adaptive
126 lymphocytes could restore ILC2 homeostasis in RAG-deficient mice. To test this, we created
127 splenocyte chimera mice by reconstituting both *Rag1*$^{-/-}$ and control WT mice with splenocytes
128 containing T and B cells from WT donor mice (**Fig. 2A**). We first assessed the overall level of
129 immune reconstitution in the recipient mice and found fully restored proportions of CD4^{+} (**Fig.**
130 **S3A**) and CD8^{+} (**Fig. S3B**) T cells in the spleens of recipient *Rag1*$^{-/-}$ mice, although B cell numbers
131 remained significantly lower than in WT mice (**Fig. S3C**). Upon induction of AD-like disease, we
132 found that the *Rag1*$^{-/-}$ mice still exhibited increased ear skin thickness (**Fig. 2B**), enhanced
133 expansion of ILC2s (**Fig. 2C**), and increased proportions of ILC2s expressing IL-5 (**Fig. 2D**) and
134 IL-13 (**Fig. 2E**) in the sdLNs. Interestingly, we found significantly higher proportions of eosinophils
135 in the spleens of *Rag1*$^{-/-}$ recipient mice (**Fig. S3D**), possibly reflecting the increased IL-5
136 production we observed from ILC2s. These findings indicate that the mere introduction of
137 exogenous T and B cells is not sufficient to suppress ILC2 dysregulation in the setting of RAG
138 deficiency.

139 To further test whether this phenotype is mediated by cell-intrinsic RAG expression, we
140 next generated mixed bone marrow (BM) chimeras. We harvested BM from congenic CD90.1^{+}
141 WT and CD90.2^{+} *Rag1*$^{-/-}$ donor mice on a CD45.2^{+} background and reconstituted sub-lethally
142 irradiated CD45.1^{+} congenic WT recipients with a 50:50 mixture of WT:*Rag1*$^{-/-}$ BM (**Fig. 2F**). After
143 confirming reconstitution of donor immune cells in the sdLN (**Fig. S4A,B**), we examined the
144 frequency and activity of ILC2s in the sdLNs based on whether they originated from WT (CD90.1^{+})
145 or *Rag1*$^{-/-}$ (CD90.2^{+}) donors (**Fig. S4C**). Strikingly, of the total donor ILC2s, the majority were
146 derived from *Rag1*$^{-/-}$ donors (**Fig. 2G**). This was not due to differences in overall donor
147 reconstitution, since measuring all Lin^{-} cells revealed WT donor cells outnumbered those from

148 *Rag1*$^{-/-}$ donors (**Fig. S4D**). Of the total IL-5- (**Fig. 2H**) and IL-13-expressing (**Fig. 2I**) ILCs, the
149 majority were also derived from *Rag1*$^{-/-}$ donors. Taken together, these data suggest that cell-
150 intrinsic RAG activity in ILC2s may limit their capacity to expand and become activated.

151

152 **A history of RAG expression marks a subpopulation of ILC2s in the skin draining lymph**
153 **node**

154 In contrast to resting naïve T cells, ILC2s resemble activated Th2 cells at steady state
155 based on their transcriptomic and epigenomic profiles[30,31]. While both T cells and ILC2s exhibit
156 historical RAG expression[23], they do not actively express the protein in their mature state[32]. Taken
157 together, these findings provoke the hypothesis that ILC2s are regulated by RAG early in
158 development to imprint alterations that influence their activity as mature cells. To distinguish ILC2s
159 as either having a history of RAG expression or not, we utilized a RAG lineage tracing system,
160 whereby a *Rag1*^{Cre} mouse was crossed to a reporter mouse expressing tandem dimer red
161 fluorescent protein (tdRFP) in a Cre-dependent manner from the *Rosa26* locus (**Fig. 3A**)[24,33]. This
162 system allowed us to compare RAG-experienced (RAG^{exp}) and RAG-naïve (RAG^{naïve}) lymphoid
163 cells, including ILC2s, simultaneously originating from the same immunocompetent host, thus
164 removing confounders inherent in knockout and chimera experiments. Analysis of sdLN from the
165 reporter mice revealed that nearly all CD4^{+} T cells, CD8^{+} T cells, and B220^{+} B cells expressed
166 tdRFP (positive history of Cre expression from the *Rag1* locus), consistent with the known
167 requirement of RAG expression for their development (**Fig. 3B-D,G**). We also examined NK cells,
168 since certain subsets of NK cells are known to express RAG during their development[24], and we
169 observed that 60% of NK cells were tdRFP^{+}, similar to previous findings (**Fig. 3E,G**)[24]. In the ILC2
170 population of the sdLN, around 50% were tdRFP^{+} (**Fig. 3F,G**), similar to proportions of RAG fate-
171 mapped ILC2s previously observed in the fat[24] and lung[23,24]. These findings demonstrate that

172 there are heterogeneous populations of ILC2s marked by differential tdRFP^{+} fate mapping.
173 Importantly, this provided us with the possibility to profile these different ILC2 subsets based on
174 *Rag1*^{Cre}-activated expression of tdRFP.

175 **Multiomic profiling enhances the detection of rare tissue-specific ILC2s**

176 Transient RAG expression early in lymphoid development leads to well-characterized,
177 durable effects on B and T cell development and function mainly through successful genomic
178 rearrangement of antigen receptors. Yet, our data indicate that RAG expression also imprints
179 phenotypic changes on ILC2s, which can develop independently of functional antigen receptors,
180 provoking the hypothesis that RAG expression may affect broader epigenomic and transcriptional
181 programs. Furthermore, our data indicate that the impact of RAG on ILC2 function has
182 implications for AD-like skin inflammation, suggesting a persistent effect that modulates
183 phenotypes of type 2 inflammation.

184 To test these hypotheses, we performed combined single-nuclei RNA sequencing
185 (snRNA-seq) and ATAC sequencing (snATAC-seq) of sdLN cells from RAG fate-mapped mice at
186 steady state and in the setting of AD-like disease (**Fig. S5A,B**). Because fluorescence-activated
187 cell sorting (FACS) can cause physical stress, cell loss, and contamination, which can introduce
188 unwanted perturbations in target cells, instead we utilized gentle initial negative selection by
189 magnetic activated cell sorting (MACS) to remove most B and T cells and monocytes prior to
190 sequencing (**Fig. S5A**). This allowed us to enrich for innate immune cell populations prior to
191 sequencing. Further, we used the gene encoding tdRFP as a barcode to differentiate between
192 RAG^{exp} (RAG fate map-positive) and RAG^{naïve} (RAG fate map-negative) ILC2s at the single-cell
193 level (**Fig. 5A**). The multiomic data was analyzed using recently developed pipelines in Cell
194 Ranger, Seurat[34–36], and Signac[37], and sequenced cells were further filtered computationally to
195 enrich for ILCs, as in previous studies (see methods)[38].

196 In addition to gene expression (GEX) information derived from snRNA-seq (**Fig. 4A**), we
197 calculated a "gene activity" (GA) score based on chromatin accessibility at gene loci (**Fig. 4B**)
198 from the corresponding snATAC-seq dataset[37]. Clustering the cells with each data subset alone
199 and in combination using weighted nearest neighbor (WNN) analysis, we identified six clusters
200 **(Fig. 4C)** that demonstrated consistent differences in cellular markers based on both metrics of
201 GEX and GA (**Fig. 4D,E; Table S1**). Additionally, top markers for each cluster clearly
202 differentiated each cell type (**Fig. 4F**). Despite successful ILC2 enrichment via MACS depletion
203 for lineage markers and computational filtering (see methods), our data set included non-ILC2
204 populations determined by gene expression to be T cells, dendritic cells, B cells, and NK cells
205 (**Fig. 4A,F; Table S1**), which allowed for broader multidimensional comparisons while studying
206 this ILC2-enriched data set.

207 To further complement the GEX and GA assays, we utilized another method of detecting
208 cell-specific marker genes, whereby chromatin regions that are differentially accessible (DA), or
209 open, in each cluster could be linked by their physical proximity to specific genes (**Fig. 4G, S6**;
210 **Table S2**; see methods). Comparing the top 100 GEX, GA, and DA markers in the ILC2
211 population, we identified a multiomic ILC2 signature of 235 unique genes (**Fig. 4H; Table S3,4**).
212 While there was some overlap between each respective set, the multiomic approach enabled
213 more extensive identification of an ILC2 gene program than through either snRNA-seq or
214 snATAC-seq alone. The analysis revealed a variety of canonical ILC2-associated genes specific
215 to the ILC2 cluster (**Fig. 4I, S6,7**) including the ILC2-activating cell surface receptors *Icos*[39,40],
216 *Il2ra*[41,42], *Il18r1*[38,43,44], *Nmur*[14,15,45–47], and *Il1rl1* (encoding the receptor for IL-33)[11,12,48,49], as well
217 as transcription factors such as *Gata3*[19,50–53], *Bcl11b*[54–57], *Maf*[19,58,59], *Ets1*[60], and *Rora*[38,51,61–63], all
218 previously shown to be important for ILC2 development and/or function.

219 Expression of some secreted proteins can be difficult to capture in droplet-based snRNA-
220 seq experiments due to low transcript levels and relatively shallow sequencing depth. With the

221 addition of the complementary GA and DA assays from snATAC-seq, our analysis identified *Il5*
222 (**Fig. 4I, S6B**), a canonical ILC2 cytokine, in the DA assay, while in the GA assay we found
223 *Bmp7*[64,65], which has been shown to be secreted by ILC2s to influence browning of adipose tissue.
224 Additionally, we identified the secreted chemokine *Ccl1* as an ILC2 marker gene[66–69], which along
225 with its cognate receptor *Ccr8* (also an ILC2 marker in our analysis)[44,67,70], participates in a feed-
226 forward circuit to drive ILC2 recruitment and expansion[71]. Thus, our findings demonstrate how
227 genetic barcoding, combining transcriptomic and epigenomic analyses, and cross-validation
228 across many published studies can yield new insights while providing internal control measures
229 to elevate the rigor, robustness, and confidence of identifying gene signatures of rare populations
230 such as ILC2s at the single-cell level.

231 **ILC2s with a history of RAG expression are epigenomically suppressed**

232 As noted above, barcoding the ILC2s afforded the opportunity to transcriptionally and
233 epigenomically profile ILC2s under identical developmental conditions by dividing the ILC2 cluster
234 into RAG^{exp} and $RAG^{naïve}$ populations. We hypothesized that RAG^{exp} ILC2s would have a distinct
235 transcriptional profile compared to ILC2s without any history of RAG expression. To test this, we
236 calculated differentially expressed genes (DEGs) for the ILC2 cluster by *Rag1* fate-map status.
237 Genes with higher expression in RAG^{exp} cells relative to $RAG^{naïve}$ cells had positive fold change
238 values, and vice versa, with genes relatively increased in $RAG^{naïve}$ cells having negative values
239 (**Fig. S8A, Table S5**). Using gene set enrichment analysis (GSEA)[72,73] on the ranked list of DEGs,
240 we found that gene sets generally representing lymphocyte activation and differentiation were
241 suppressed in RAG^{exp} ILC2s compared to $RAG^{naïve}$ ILC2s (**Fig. S8B,C, Table S6**), consistent with
242 our previous observations that ILC2s are expanded and more activated in RAG-deficient mice
243 relative to WT mice.

244 We next employed newly described methodologies[37,74] that quantify associations between
245 open chromatin peaks and the expression of nearby genes to describe the functional regulomes

246 of both RAG^{exp} and RAG^{naïve} ILC2s (**Fig. 5B**). In this analysis, each ATAC peak can be linked to
247 multiple genes, and each gene to multiple peaks, generating a list of "gene-to-peak links" or GPLs
248 (see methods). For each gene, we interpreted the number of corresponding GPLs as a
249 quantitative representation of the regulome activity for that gene. Considering RAG^{exp} and
250 RAG^{naïve} cells as two separate populations, we generated two lists of GPLs (**Table S7**) defining
251 functional regulomes for each population. We focused our analysis on the functional regulomes
252 of ILC2s by filtering the GPL lists for the 235 unique ILC2 genes identified in our multiomic gene
253 set (**Fig. 4H; Table S8**), then calculated the difference in GPLs between RAG^{exp} and RAG^{naïve}
254 cells for each gene and sorted them; genes displaying greater numbers of GPLs in the RAG^{naïve}
255 population are at the top, and genes with more GPLs in the RAG^{exp} population are at the bottom
256 (**Fig. 5C; Table S9**).

257 We found that the ILC2 marker genes segregating toward the top of this list, corresponding
258 to enhanced epigenomic activity in the RAG^{naïve} cells, tended to be genes previously identified to
259 play positive roles in development, expansion, and activation of lymphoid cells. These included
260 transcriptional regulators such as *Tox*[75–78], *Rora*[38,51,61–63], *Maf*[19,58,59], and *Gata3*[19,50–52], which are
261 involved in early differentiation of both ILCs and lymphocytes (**Fig. S9A**). Indeed, epigenetic
262 activation of the *Gata3* locus is recognized to play a critical role in development of both ILC2s[79]
263 and Th2 cells[80,81]. Additionally, surface receptors known to drive ILC2 activation upon stimulation
264 including *Il18r1*[38,43,44], *Il1rl1*[21,38,43,82,83], and *Icos*[39,40] had increased functional regulome activity in
265 RAG^{naïve} ILC2s. In contrast, genes with more GPLs in the RAG^{exp} ILC2s tended to be associated
266 with suppressive functions. For example, *Ndfip1* (**Fig. S9B**) encodes a regulatory protein that
267 enhances activity of the ubiquitin ligase ITCH to negatively regulate inflammation[84,85] and has
268 been associated with asthma risk in GWAS studies[86]. *Dusp1* partially mediates glucocorticoid
269 effects through its ability to negatively regulate inflammation[87,88], is associated with eczema by
270 GWAS[89], and has recently been shown to mark an anti-inflammatory set of ILCs[69]. Last, *Asxl1*

271 encodes a tumor suppressor that inhibits clonal hematopoiesis through its epigenomic regulatory
272 effects in both mice and humans[90–93]. Collectively, our GPL analysis stratifies the ILC2 gene
273 signature based on RAG experience, where genes associated with ILC2 expansion and activation
274 are poised in RAG^{naïve} cells, while genes associated with suppressive effects are poised in RAG^{exp}
275 cells.

276 **A history of RAG expression modulates ILC2 epigenomes at steady state and in AD-like**
277 **inflammation**

278 Although our GPL analysis revealed a suppressive effect of RAG expression on ILC2 gene
279 programs, we did not account for the additional variable of disease state in the initial analysis. To
280 test whether RAG expression promotes a suppressive epigenomic program in ILC2s that is
281 durable in the setting of inflammation, we first recalculated GPLs after splitting our dataset by both
282 history of RAG expression (naïve vs. experienced) and disease (steady state vs. AD-like disease)
283 to yield four lists of GPLs (**Fig 6A; Table S10**). When we examined the intersection, or overlap,
284 of peaks from ILC2 GPLs (**Table S11**), several notable patterns emerged (**Fig. 6B**). First, the
285 largest set of peaks was shared by all RAG^{naïve} cells (gray bar), regardless of disease state, with
286 the next largest peak sets belonging to either steady state or AD-like disease in the RAG^{naïve} cells.
287 Second, there was a large set of peaks shared by all RAG^{exp} cells (red bar). Third, the
288 intersections corresponding to disease states (steady state – yellow, AD-like disease – dark red),
289 had relatively few unique peaks. These findings suggest that early exposure to RAG expression
290 plays a larger role in modulating the epigenomic signature of the ILC2 gene program than
291 exposure to disease. To confirm that the patterns we observed represent a specific effect of RAG
292 expression on the ILC2 gene program, we performed the same analysis on GPL peaks for all
293 genes in the dataset (**Fig. S10**). In contrast to the ILC2 gene set, the majority of GPL peaks for
294 all genes was shared among all cell populations, consistent with epigenomic regulation of most
295 genes being minimally affected by either RAG expression or AD-like disease. Last, in the ILC2
296 gene set analysis, we noted a set of poised peaks shared by all RAG^{naive} cells and RAG^{exp} cells

297 in the setting of AD-like disease, but not with RAG^{exp} cells at steady state (blue bar, **Fig. 6B**). We
298 reasoned that this condition might capture some genomic loci that are suppressed by a history of
299 RAG expression at steady state but are induced during inflammation.

300 Thus, we next quantified and sorted these GPLs to generate a list of genes with the most
301 peaks "induced" during AD-like disease (**Fig. 6C, Table S12**). Among the identified genes, we
302 selected *Rora* (**Fig. 6C**) and *Ccr6* (**Fig. 6D**) to examine more closely for evidence of epigenomic
303 activation in AD-like disease, given the role of these genes in ILC2 expansion[61,62] and homing to
304 sites of inflammation[44,94], respectively. For both genes, we observed more widespread open
305 chromatin over the genomic region in the RAG^{naïve} cells compared to the RAG^{exp} cells, but this
306 difference was partially abolished by increased open chromatin in AD-like disease in the RAG^{exp}
307 cells. Taken together, our analysis reveals that a history of RAG expression selectively modulates
308 activity of ILC2 gene programs across both steady state and during AD-like inflammation, while
309 some programs are more evident at steady state given the uniquely poised nature of ILC2s.

310 **RAG suppresses the Th2 locus**

311 Our functional data demonstrate a role for RAG expression in regulating ILC2
312 development and activation, including limiting proportions of IL5^{+} and IL-13^{+} ILC2s at steady state
313 and in AD-like disease. Prior work identified epigenomic priming in ILC2s early in development at
314 the Th2 locus (comprised of the *Il4*, *Il13*, *Rad50*, and *Il5* gene loci) to enable rapid transcriptional
315 responses during inflammation[30]. Thus, we hypothesized that RAG promotes the functional
316 observations in ILC2s by suppressing the establishment of an active regulome at the Th2 locus.
317 To test this hypothesis, we analyzed the Th2 locus in our multiomic data in greater detail. Using
318 a similar strategy to our analysis of ILC2 marker genes, we calculated the number of GPLs in the
319 RAG^{exp} and RAG^{naïve} cells, respectively, for the genes in the Th2 locus. (**Fig. 7A, Table S7**). We
320 found many GPLs associated with the four Th2 locus genes, including significant crosstalk
321 *between* these genes, similar to previous observations (**Fig. 7A**)[95–97]. Importantly, we identified

322 fewer GPLs in the RAG^{exp} cells, particularly for the *Il5* and *Il13* loci (**Fig. 7A**). As in our analysis
323 of the ILC2 marker GPLs, we quantified the differences based on RAG fate mapping and found
324 that all genes in this locus had increased GPLs in RAG^{naïve} cells relative to RAG^{exp} cells (**Fig. 6B;**
325 **Table S13**). Thus, our epigenomic data are consistent with a role for RAG expression in
326 suppressing the type 2 regulome at the Th2 locus in ILC2s.

327 We next considered the additional effects of AD-like inflammation on the Th2 epigenomic
328 regulome using the same approach we used to analyze the ILC2 gene set in **Fig. 6**. Again, we
329 found the largest set of peaks was shared by the RAG^{naïve} cells, regardless of disease state, with
330 the next largest peak sets belonging to either steady state or AD-like disease in the RAG^{naïve} cells
331 (**Fig. 7C**). Furthermore, there was a large proportion of peaks shared by both RAG^{exp} cells,
332 consistent with a major contribution of a history of RAG expression to epigenomic modulation of
333 the Th2 regulome. To quantify the potential effect of AD-like inflammation on reversing RAG-
334 mediated suppression of Th2 locus genes, we mapped the 14 peaks shared by RAG^{naive} cells and
335 RAG^{exp} cells in the setting of AD-like inflammation (i.e. only suppressed in RAG^{naive} cells at steady
336 state) back to the Th2 genes via their respective GPLs (**Fig. 7C - blue bar, Table S14**).
337 Interestingly, *Il13*, which was not identified as a top ILC2 marker in our earlier analyses, had the
338 highest number of linked peaks associated with potential induction in AD-like disease (**Fig. 7D**).
339 When we examined the *Il13* locus in the ILC2 cluster more closely, we found more widespread
340 open chromatin in the RAG^{naïve} cells compared to the RAG^{exp} cells (**Fig. 7E**). However, in the AD-
341 like disease sample, the RAG^{exp} cells displayed increased open chromatin relative to the steady
342 state, consistent with induction in the setting of inflammation, like our earlier findings for ILC2
343 genes such as *Ccr6* (**Fig. 6E**). Taken together, our functional data and multiomic analyses
344 demonstrate a role for RAG expression in modulating genes critical for ILC2 development and
345 function, including the key type 2 cytokines expressed from the Th2 locus.

346

347 **DISCUSSION**

348 RAG recombinases evolved nearly 500 million years ago from endogenous transposons,
349 crucially enabling antigen receptor rearrangement and emergence of the adaptive immune cell
350 lineages present in all modern vertebrates[29,98]. Indeed, RAG deficiency leads to a complete lack
351 of B and T lymphocytes, manifesting clinically as severe combined immunodeficiency (SCID)[99–
352 101]. However, fate mapping studies have shown that multiple mature immune cell populations
353 other than adaptive B and T lymphocytes have a history of RAG expression[23,24,33,102,103]. More
354 recent studies by Karo et al found that RAG expression during NK cell development influences
355 multiple cellular functions including antitumor cytotoxicity, cell proliferation, and survival[24]. Yet
356 whether RAG modulates cellular functions of innate immune cell populations other than NK cells
357 remains poorly understood. Here, using RAG-deficient mice, RAG fate mapping mice, and
358 multiomic analyses, we report that RAG suppresses developmental and effector functions of
359 ILC2s.

360 Our functional data in RAG-deficient mice demonstrate that populations of ILC2s
361 producing the type 2 cytokines IL-5 and IL-13 preferentially expand in the absence of a history of
362 RAG expression. This implies a specific role for RAG in developmental repression of ILC2s.
363 Building on this, our multiomic RAG fate mapping analyses of ILC2 gene programs demonstrate
364 extensive epigenomic differences between RAG^{exp} and $RAG^{naïve}$ cells. We found RAG-associated
365 epigenomic suppression at multiple functional levels, including cell surface receptors, key
366 transcription factors, and the Th2 locus encoding the type 2 cytokines *Il5* and *Il13*. Although RAG
367 is only transiently expressed early in lymphoid development[104], our data demonstrate that RAG
368 expression can imprint durable effects on ILC2 gene programs to restrain their function.

369 It is increasingly recognized that expression of effector molecules for both ILCs and their
370 counterpart adaptive lymphocytes (e.g. IL-13 from ILC2s and Th2 cells) is governed by finely

371 tuned transcriptomic and epigenomic regulomes[30,105–107]. ILCs tend to adopt these regulomes
372 earlier in their development than T cells, and these “poised” regulatory elements are thought to
373 underlie the ability of tissue-resident ILCs to rapidly respond to stimuli. In contrast, the regulomes
374 of naïve T cells remain relatively inactive until stimulation. Given that T cells are uniformly RAG-
375 experienced, our data provoke the hypothesis that RAG^{exp} ILC2s adopt a phenotype closer to that
376 of naive T cells and may require stronger stimuli than $RAG^{naïve}$ ILC2s to become activated. Indeed,
377 our analyses found the RAG-associated suppressive programs could be overcome in the setting
378 of AD-like inflammation. Thus, sufficient RAG expression may mediate key events underlying the
379 establishment and maintenance of functional regulomes not only in ILCs, but also T cells. How
380 RAG might affect these changes, and whether they are independent of its enzymatic activity
381 and/or antigen receptor recombination, remains to be elucidated.

382 Clinically, a link between enhanced type 2 immune activity and RAG dysfunction is well-
383 established. Omenn Syndrome (OS) is a form of SCID characterized by exaggerated type 2
384 immune activation and typically arises in the setting of hypomorphic RAG gene mutations.
385 Impaired antigen receptor rearrangement, with rare “leaky” recombination events, leads to
386 expansion of autoreactive oligoclonal T cells, eosinophilia, and markedly elevated IgE[108–112].
387 Similar phenotypes have been observed in mice harboring RAG mutations analogous to those
388 found in human patients with OS[113,114]. Notwithstanding these findings, the mechanisms
389 underlying the propensity of oligoclonal T cells with hypomorphic RAG activity to preferentially
390 develop into the Th2 subtype are unclear. Prior studies have found a role for regulatory T cells in
391 controlling type 2 skewing of transferred T cells in RAG-deficient hosts, potentially explaining
392 similar observations in patients with OS[115]. Our data provide an additional mechanism by which
393 RAG dysfunction may lead to OS through loss of cell-intrinsic RAG-mediated suppression of type
394 2 cellular programs. Additionally, increased type 2 cytokine production from RAG-deficient ILC2s
395 may, in *trans*, enhance expansion of the oligoclonal Th2 cell populations, IgE induction, and

396 eosinophilia observed in RAG-deficient states like OS. However, whether other immune cell types
397 with RAG dysfunction, such as ILCs, contribute to the pathogenesis of OS in humans has not
398 been investigated.

399 Lymphoid acquisition of RAG activity may represent a newer evolutionary mechanism that
400 fine tunes ancient innate immune cell programs in addition to enabling development of relatively
401 newer antigen-specific adaptive immune cell populations. Independent of antigen receptor
402 diversity, loss of this function may offer an explanation as to why oligoclonal T cells tend to expand
403 and skew towards a Th2 cell phenotype in the setting of hypomorphic RAG function as in OS[115].
404 Further studies are needed to define whether the suppressive effects of RAG expression operate
405 similarly in T and B cells. Although we demonstrate that this phenomenon is observed in ILC2s,
406 whether hypomorphic RAG expression in bona fide Th2 cells not only results in oligoclonality but
407 also loss of suppression of the Th2 locus independently of antigen receptor rearrangement
408 remains an outstanding question. Indeed, during development of gene therapy strategies for
409 RAG-deficient SCID, lower doses of wild type RAG transgene expression have been associated
410 with development of OS-like conditions in transplanted RAG-deficient mice[116–119].

411 A major limitation of our study is lack of a defined mechanism for how RAG expression
412 imprints durable epigenomic and transcriptomic changes in ILC2s. The mechanisms by which
413 RAG mediates VDJ recombination are well-defined, from the biochemical details of DNA-binding
414 to the epigenomic accessibility of antigen receptor loci and timing of RAG expression[29,120–122].
415 Notwithstanding genomic stress[24] or potential RAG dose effects[116–119], how RAG expression
416 might modulate broad developmental and functional lymphoid programs other than V(D)J
417 recombination remains unclear. The RAG complex can bind both DNA and modified histones and
418 has been observed to occupy thousands of sites across the genome[27]. Thus, RAG may directly
419 influence open chromatin states or obscure transcription factor binding sites to alter ILC2
420 development and function. Interestingly, RAG preferentially binds near transcription start sites of

open chromatin in mouse pre-B cells, although corresponding effects on gene expression were not observed[27]. Although canonical recombination sites are concentrated in the antigen receptor loci, cryptic recombination sites in other regions may be deleted or rearranged by RAG activity, altering transcriptional regulation of associated genes[27]. Finally, through its E3 ubiquitin ligase activity[29], RAG may influence immune signaling pathways independently of transcription altogether. Beyond basic mechanisms of how RAG modulates ILC2 development and function, whether these effects may contribute to pathologic processes modulated by ILC2s in organs other than the skin remains unclear.

Our studies expand prior work implicating RAG in critical immune functions beyond antigen receptor rearrangement that is exclusive to adaptive lymphocytes. Further, we provide additional insights into why patients with OS exhibit atopic syndromes in the setting of adaptive lymphocyte deficiency. Future studies into mechanisms underlying these findings may lead to new therapeutic avenues for disorders such as atopic dermatitis, food allergy, and asthma.

ACKNOWLEDGEMENTS

We thank all members of the Kim lab for helpful comments and discussion. This work is supported by the Allen Discovery Center program, a Paul G. Allen Frontiers Group advised program of the Paul G. Allen Family Foundation, the Doris Duke Charitable Foundation, LEO Pharma, the National Institute of Arthritis and Musculoskeletal and Skin Diseases (NIAMS) (AR070116, AR077007, and AR080392), and the National Institute of Allergy and Infectious Disease (NIAID) (AI167933 and AI167047) of the National Institutes of Health (NIH). A.M.V. is supported by NIAMS (1K08AR080219). M.T. is supported by the Japanese Society of Allergology (JSA) International Scholarship. A.M.T. is supported by the NIAID (AI007163 and AI154912). We thank the Genome Technology Access Center at the McDonnell Genome Institute at Washington

University School of Medicine for help with genomic analysis. The Center is partially supported by NCI Cancer Center Support Grant #P30 CA91842 to the Siteman Cancer Center and by ICTS/CTSA Grant# UL1TR002345 from the National Center for Research Resources (NCRR), a component of the National Institutes of Health (NIH), and NIH Roadmap for Medical Research. This publication is solely the responsibility of the authors and does not necessarily represent the official view of NCRR or NIH.

AUTHOR CONTRIBUTIONS

Conceptualization: A.M.V., M.M., L.Z., M.T., T-L.Y., and B.S.K.

Methodology: A.M.V., M.M., M.T., L.Z., T-L.Y., and B.S.K.

Validation: A.M.V., M.M., L.Z., M.T., and T-L.Y.

Formal Analysis: A.M.V. and M.M.

Investigation: A.M.V., M.M., L.Z., M.T., T-L.Y., D-H.K., and H.J-M.

Resources: S.V.D. and B.S.K.

Writing – Original Draft: A.M.V.

Writing – Review & Editing: All authors

Supervision, B.S.K.

Funding Acquisition, B.S.K.

464 **DECLARATION OF INTERESTS**

465 B.S.K. is founder of Alys Pharmaceuticals; he has served as a consultant for 23andMe,
466 ABRAX Japan, AbbVie, Amgen, Cara Therapeutics, Clexio Biosciences, Eli Lilly and Company,
467 Escient Pharmaceuticals, Evommune, Galderma, Genentech, LEO Pharma, Pfizer, Recens
468 Medical, Regeneron, Sanofi, Septerna, Triveni Bio, and WebMD; he has stock in ABRAX Japan,
469 Alys Pharmaceuticals, Locus Biosciences, and Recens Medical; he holds a patent for the use of
470 JAK1 inhibitors for chronic pruritus; and he has a patent pending for the use of JAK inhibitors for
471 interstitial cystitis. A.M.V. has contributed to scientific advisory boards at Galderma and has
472 performed sponsored research for Amgen.

473

474 **FIGURE TITLES AND LEGENDS**

475 **Figure 1: RAG deficiency leads to expansion and activation of ILC2s during inflammation**
476 **and at steady state.**

477 **A)** Experimental schematic of AD-like disease. WT (Control) B6 mice or *Rag1*$^{-/-}$ mice treated
478 topically to the inner surface of each ear with 2 nmol MC903 in 10 μL ethanol vehicle daily for 7
479 days develop AD-like inflammation. **B)** Ear thickness measured daily in AD-like inflammation.
480 Data representative of at least 2 independent experiments, 5 mice/group. ** $P < 0.01$ by 2-way
481 ANOVA with Sidak's multiple comparisons test, day 7. **C)** Proportion of CD90^{+}, Lin^{-} cells (Lin^{-}
482 defined as CD3^{-}, CD5^{-}, CD11b^{-}, CD11c^{-}, CD19^{-}, NK1.1^{-}, and FcεR1^{-}) determined to be ILC2s (IL-
483 33R^{+}) in skin-draining lymph nodes (sdLN) from WT or *Rag1*$^{-/-}$ mice with AD-like ear inflammation.
484 Percent ILC2 from sdLN in AD-like disease following PMA/iono stimulation positive for **D)** IL-5 or
485 **E)** IL-13 staining. **F)** Schematic of steady state analysis of sdLN from WT (Control) or *Rag1*$^{-/-}$ mice.
486 **G)** Proportion of steady state sdLN CD90^{+}, Lin^{-} cells determined to be ILC2s as in **(C)**. Percent
487 ILC2 from sdLN in steady state following PMA/iono stimulation positive for **H)** IL-5 or **I)** IL-13
488 staining. **C-E; G-I)** Data representative of at least 2 independent experiments, 4-5 mice/group * P
489 < 0.05, ** $P < 0.01$, *** $P < 0.001$ by two-tailed Welch's t test. All data represented as mean with
490 standard deviation.

491

492 **Figure S1: ILC2 and IL-5/IL-13 gating.**

493 Gating for **A)** CD45^{+}, CD90^{+}, Lin^{-} cells (Lin^{-} defined as CD3^{-}, CD5^{-}, CD11b^{-}, CD11c^{-}, CD19^{-},
494 NK1.1^{-}, and FcεR1^{-}), then gating on **B)** ILC2 (IL-33R^{+} Lin^{-}) corresponding to **Fig. 1C**, with
495 subsequent gating of **C)** IL-5^{+} and IL-13^{+} ILC2, corresponding to **Fig. 1D-E.**

496

497 **Figure S2: Expansion and activation of ILC2s in RAG2 deficiency compared to littermates.**

498 **A)** Schematic of steady state analysis of WT B6 (Control) mice or *Rag2*$^{-/-}$ mice. **B)** Proportion of
499 CD90^{+} Lin^{-} cells (Lin- defined as CD3^{-}, CD5^{-}, CD11b^{-}, CD11c^{-}, CD19^{-}, NK1.1^{-}, and FcεR1^{-})
500 determined to be ILC2s (IL-33R^{+}) in sdLN at steady state from WT or *Rag2*$^{-/-}$ mice. Percent ILC2
501 from sdLN at steady state following PMA/iono stimulation positive for **C)** IL-5 or **D)** IL-13 staining.
502 Data representative of 2 independent experiments, 2-3 mice per group. * P <0.05, ** P < 0.01 by
503 two-tailed Welch's t test. All data represented as mean with standard deviation.
504
505 **Figure 2: Homeostatic expansion and activation of RAG-deficient ILC2s is cell intrinsic**
506 **A)** Experimental schematic of AD-like disease in splenocyte chimera experiment. WT B6 or *Rag1*$^{-}$
507 $^{/-}$ mice received WT splenocytes and developed AD-like inflammation after subsequent topical
508 treatment with 2 nmol MC903 in 10 µL ethanol vehicle to each ear daily for 10 days. **B)** Ear
509 thickness measured daily in AD-like inflammation. Data representative of 2 independent
510 experiments, 4-5 mice per group. **** P <0.0001 by 2-way ANOVA with Sidak's multiple
511 comparisons test, day 10. **C)** Proportion of CD90^{+}, Lin^{-} cells (Lin^{-} defined as CD3^{-}, CD5^{-}, CD11b^{-}
512 , CD11c^{-}, CD19^{-}, NK1.1^{-}, and FcεR1^{-}) determined to be ILC2s (IL-33R^{+}). Percent ILC2 from sdLN
513 in splenocyte chimera mice with AD-like disease after PMA/iono stimulation positive for **D)** IL-5 or
514 **E)** IL-13 staining. **F)** Schematic of bone marrow chimera experiment. Equal quantities of bone
515 marrow cells from *Rag1*$^{-/-}$ (CD45.2, CD90.2 - orange) and WT (CD45.2, CD90.1 - blue) C57Bl/6J
516 donor mice were used to reconstitute the immune systems of irradiated recipient WT (CD45.1 -
517 black) C57Bl/6J mice. **G)** Proportion of donor (CD45.2^{+}) ILC2 defined as in (C) in sdLN by donor
518 source (CD90.1^{+} - WT, CD90.2^{-} - *Rag1*$^{-/-}$). Proportion of Lin^{-} ILCs by donor source positive for **H)**
519 IL-5 and **I)** IL-13 following PMA/iono stimulation and cytokine staining. **C-E)** Data representative
520 of at least 2 independent experiments, 4-5 mice per group. ** P < 0.01, **** P < 0.0001 by two-
521 tailed Welch's t test. **G-H)** Data representative of at least 2 independent experiments, 4-5 mice
522 per group. ** P < 0.01 by two-tailed ratio means paired t test. All data represented as mean with
523 standard deviation.

524

525 **Figure S3: Confirmation of splenocyte reconstitution in splenocyte chimera mice.**

526 Proportion of $CD45^+$ splenocytes from splenocyte chimera mice (related to **Fig. 2A-E**) determined

527 to be **A)** $CD4^+$ T cells ($CD4^+$, $CD8^-$, $CD19^-$), **B)** $CD8^+$ T cells ($CD4^-$, $CD8^+$, $CD19^-$), **C)** B cells ($CD4^-$

528 , $CD8^-$, $CD19^+$), and **D)** Eosinophils ($SiglecF^+$, $CD4^-$, $CD8^-$).

529

530 **Figure S4: Donor cell reconstitution and gating in sdLN of WT:*Rag1*$^{-/-}$ bone marrow chimera**

531 **mice.**

532 **A)** Gating of live host ($CD45.1^+$) and donor ($CD45.2^+$) cells and **B)** quantification in sdLN of

533 WT:*Rag1*$^{-/-}$ bone marrow chimera mice. ** $P < 0.01$, **** $P < 0.0001$, by RM one-way ANOVA test

534 with Geisser-Greenhouse correction.

535 **C)** Gating, and **D)** quantification of $CD45.2^+$ Lin^- donor cells by genotype (WT - blue and *Rag1*$^{-/-}$ -

536 orange) in sdLN of WT:*Rag1*$^{-/-}$ bone marrow chimera mice. * $P < 0.05$ by ratio means paired t

537 test. All data represented as mean with standard deviation. Related to **Fig. 2F-I.**

538

539 **Figure 3: A history of RAG expression marks a population of ILC2s in the sdLN.**

540 **A)** Schematic of RAG fate mapping in the lymphoid cell compartment using reporter mice

541 expressing Cre-inducible tandem dimer red fluorescent protein (tdRFP) from the *Rosa26* locus

542 crossed to mice expressing Cre recombinase from the *Rag1* locus. **B-F)** Histograms of tdRFP

543 signal in $CD45^+$ sdLN cells by cell type for **B)** $CD4^+$ T cells ($B220^-$, $CD3^+$, $CD4^+$), **C)** $CD8^+$ T cells

544 ($B220^-$, $CD3^+$, $CD8^+$), **D)** B cells ($MHCII^+$, $B220^+$), **E)** NK cells ($B220^-$, $CD3^-$, $CD4^-$, $CD8^-$, $CD49b^+$,

545 $NK1.1^+$), **F)** ILC2s ($B220^-$, $CD3^-$, $CD4^-$, $CD8^-$, $CD49b^-$, $NK1.1^-$, $CD11b^-$, $CD11c^-$, $SiglecF^-$, $CD90^+$,

546 $KLRG1^+$ or $ICOS^+$ or $IL\text{-}33R^+$), **F)** quantification of $tdRFP^+$ proportion of each cell type.

547

548

549

550 **Figure S5: sdLN multiome experiment.**

551 **A)** *Rag1*^{Cre}::*Rosa26*$^{LSL\text{-}tdRFP}$ reporter mice were given topical treatments with 2 nmol MC903
552 dissolved in ethanol vehicle or with ethanol vehicle alone to each ear daily for 7 days. Harvested
553 sdLN processed using Magnetic Activated Cell Sorting (MACS) led to depletion of cells
554 expressing the CD3, CD19, and CD11b lineage markers and remaining cells were further
555 processed in the 10X Multiome pipeline, generating both single cell RNA-sequencing and single
556 cell ATAC-sequencing data for each cell. **B)** Ear thickness measured daily in the AD-like disease
557 multiome experiment. Data representative of one experiment, with 4 mice per group pooled for
558 sequencing. **** P <0.0001 by 2-way ANOVA with Sidak's multiple comparisons test, day 7. All
559 data represented as mean with standard deviation.

560

561 **Figure 4: Multiomic analysis of ILC2s through single nuclei sequencing of the sdLN.**

562 **A)** Schematic of the gene expression (GEX) assay derived from snRNA-seq data. **B)** Schematic
563 of the gene activity (GA) assay, representing estimated transcription scores derived from
564 snATAC-seq data using Signac. **C)** UMAP visualizations of independent analyses of RNA-seq
565 and ATAC-seq data for 2034 sdLN cells after dimensional reduction and clustering combined
566 using weighted nearest neighbor (WNN) analysis in Seurat. Cluster identities are color coded
567 consistently throughout the following panels. Heatmaps of **D)** top 25 GEX marker genes and **E)**
568 top 25 GA marker genes identified for each cluster. See **Table S1** for full lists of genes. **F)** Dotplots
569 comparing selected marker genes for each cluster between the GEX and GA assays, with
570 emphasis on known cell type-specific markers. **G)** Schematic of differentially accessible (DA)
571 chromatin assay, which finds the nearest gene to any peak calculated to be differentially open in
572 a particular cell cluster. See **Table S2** for full lists of top 25 DA cluster markers. **H)** Overlap of top
573 100 markers for the ILC2 cluster from the GEX, GA, and DA assays. See **Table S3** for top 100
574 DA peaks and distances to nearest genes and **Table S4** for full list of top 100 ILC2 markers. **I)**
575 Selected genes from the ILC2 gene set for each assay individually and for overlaps.

576

577 **Figure S6: ILC2 marker genes identified in the differentially accessible open chromatin**
578 **assay.**

579 Differentially accessible (DA) open chromatin peaks identified for the ILC2 cluster are highlighted
580 in gray and shown next to the closest gene for **A)** Neuromedin U receptor 1 (*Nmur1*) and **B)** IL-5
581 (*Il5*). See **Table S3** for top 100 DA peaks and distances to nearest genes for the ILC2 cluster.

582

583 **Figure S7: Dotplots of selected ILC2 marker genes.**

584 Dotplots comparing selected marker genes from the multiomic ILC2 gene set (**Figure 4I, Table**
585 **S4**) for each cluster between the GEX and GA assays, with genes highlighted by color
586 corresponding to individual assays or overlap of assays in which they were identified. *Rora* was
587 not detected in the GA assay.

588

589 **Figure 5: A history of RAG expression imprints transcriptomic and epigenomic modulation**
590 **of ILC2 gene programs.**

591 **A)** Schematic of transcriptional RAG fate mapping. Sequenced cells from the RAG fate map
592 mouse (see Figure 3A) transcribe tdRFP only after Cre is expressed from the *Rag1* locus. Cells
593 were assigned as either having a history of RAG expression (RAG^{exp} - tomato red) or not ($RAG^{naïve}$
594 - dark gray) based on detection of tdRFP transcript in the RNA-seq data. **B)** Schematic of mapping
595 gene to peak links (GPLs). The LinkPeaks function of Signac (see methods) calculates significant
596 correlations between open chromatin at defined peaks (teal bars) and nearby gene expression.
597 These links represent inferred epigenomic-transcriptomic regulation, or "regulomes" based on the
598 correlated snRNA- and snATAC-sequencing data. After calculating GPLs separately for each
599 population (gray for $RAG^{naïve}$ and tomato red for RAG^{exp}), GPLs found in only one group, but not
600 the other, can be identified (teal boxes). The difference in GPLs based on RAG experience for
601 any given gene (e.g. Gene X) can be visualized on a bar graph, with the number of GPLs for

602 RAG^{naïve} (gray - left) and RAG^{exp} (red - right) plotted, with the difference overlaid as a black bar.
603 **C)** GPLs calculated as in (B) for the multiomic ILC2 gene set identified in **Figure 4H** and **Table**
604 **S4**). All identified GPLs are listed in **Table S7**, while ILC2 GPLs are listed in **Table S8**. Genes are
605 sorted from more links identified in the RAG^{naïve} population at top to more links identified in the
606 RAG^{exp} population at bottom. Select genes are labeled. Full ranked list by difference in GPLs is
607 available in **Table S9**.
608
609 **Figure S8: Gene set enrichment analysis of differentially expressed genes in ILC2s.**
610 **A)** Volcano plot of differentially expressed genes (DEGs) by RAG fate map for the ILC2 cluster.
611 A ranked list (**Table S5**) was constructed for all DEGs with $\log_2$(fold change) >0.1 for gene set
612 enrichment analysis (GSEA). **B)** Dotplot of GSEA result calculated using ClusterProfiler and the
613 gene ontology (GO) biological process (BP) database (see methods). Full results in **Table S6**. **C)**
614 GSEA plot of the GO BP "positive regulation of immune system process" gene set. RAG^{naïve}, RAG
615 fate map negative; RAG^{exp}, RAG fate map positive.
616
617 **Figure S9: Mapping gene to peak links in select ILC2 genes.**
618 Gene to peak links (GPLs) mapped for the RAG^{naïve} and RAG^{exp} states as depicted in **Figure 5B**
619 for **A)** GATA binding protein 3 (*Gata3*) and **B)** Nedd4 family interacting protein 1 (*Ndfip1*). Only
620 GPLs that fit in the coverage window are shown. Select peaks (teal bars) present in one state,
621 but not the other, are highlighted in teal boxes. Full gene names not shown on figure in (A) are
622 **9230102O04Rik* and ***4930412O13Rik* and in (B) #*Gm42690*.
623
624 **Figure 6: A history of RAG expression broadly influences ILC2 genes at steady state and**
625 **in AD-like inflammation.**
626 **A)** Schematic of the process to determine contribution of RAG fate map and disease states to
627 GPLs for subsequent intersection analyses. GPLs were first calculated for all indictated cells,

628 regardless of disease state or fate map. Cells were then split, first by RAG fate map (RAG^{exp} and
629 $RAG^{naïve}$), and again by disease state (SS - steady state, AD - AD-like inflammation). GPLs were
630 recalculated for each split sample and matched back to the original set of total GPLs. **B)** UpSet
631 plot visualizing intersections of peaks identified from ILC2 GPLs for split samples. Each row
632 represents one of the four sets, and each column corresponds to an intersection of one or more
633 sets (see methods). See **Table S10** for full list of GPLs for all genes. **Table S11** lists total and
634 ILC2 peaks used for intersection analyses in each of the four sets. Columns identifying key
635 intersections are color coded by the corresponding RAG fate map or treatment groups. The blue
636 column indicates the intersection of peaks from $RAG^{naïve}$ cells and peaks induced by AD-like
637 disease in RAG^{exp} cells. **C)** Top genes with the most AD-like disease-induced peaks. Peaks from
638 the intersection between $RAG^{naïve}$ cells and inflamed RAG^{exp} cells were identified in corresponding
639 GPLs, and genes were ranked by number of linked peaks identified. See **Table S12** for full list of
640 ranked genes and associated GPLs. Open chromatin in the ILC2 cell cluster split by disease state
641 and then by RAG fate map for the genomic loci of **C)** *Ccr6* and **D)** *Rora*.
642
643 **Figure S10: Gene to peak link analysis by RAG fate map and disease for all detected genes.**
644 **A)** UpSet plot of overlaps in peaks identified from GPLs of all genes split by both RAG fate map
645 (RAG^{exp} and $RAG^{naïve}$) and disease state (SS - steady state, AD - AD-like inflammation). Each row
646 corresponds to one of the four sets, and each column corresponds to an intersection of one or
647 more sets (see methods). See **Table S11** for full list of peaks from GPLs for all genes in each set.
648 Columns identifying key intersections are color coded by the corresponding RAG fate map or
649 disease groups. The blue column indicates the intersection of peaks from $RAG^{naïve}$ cells and
650 peaks induced by AD-like disease in RAG^{exp} cells.
651
652
653

654 **Figure 7: RAG suppresses the Th2 locus.**

655 **A)** Coverage plot of the Th2 genomic locus. Open chromatin in the ILC2 cluster for each *Rag1*
656 fate-mapped state is shown on top, and corresponding peaks (teal) and gene to peaks links
657 (GPLs) are shown below for the $RAG^{naïve}$ sample (gray) and the RAG^{exp} sample (tomato red).
658 Only GPLs that fit in the coverage window are shown. **B)** All GPLs identified in each fate map
659 state for the Th2 locus genes *Il4*, *Il13*, *Rad50*, and *Il5*. See **Table S13** for full list of Th2 GPLs.
660 The number of GPLs for each gene is shown on the left in gray for $RAG^{naïve}$ and on the right in
661 tomato red for RAG^{exp}. The difference is superimposed in black, and genes are sorted from more
662 GPLs identified in $RAG^{naïve}$ at top to more links identified in RAG^{exp} at bottom. **C)** UpSet plot of
663 intersections of peaks identified from Th2 locus GPLs. GPLs were recalculated, this time for
664 samples separately by both RAG fate map status (RAG^{exp} and $RAG^{naïve}$) and disease (SS - steady
665 state, AD - AD-like inflammation). Each row represents one of the four sets of peaks, and each
666 column corresponds to an intersection of one or more sets (see methods). See **Table S11** for full
667 list of peaks from GPLs for all genes, including Th2 genes, in each of the four sets. Columns
668 identifying key intersections are color coded by the corresponding RAG fate map or disease
669 groups. The blue column indicates the intersection of peaks from $RAG^{naïve}$ cells and peaks
670 induced in AD-like disease in RAG^{exp} cells. (**D)** Th2 genes sorted by number of AD-like disease-
671 induced peaks. Peaks induced by AD-like disease were identified in corresponding GPLs, and
672 genes were ranked by frequency of links to induced peaks (representation in identified GPLs).
673 See **Table S14** for full list of ranked Th2 locus genes and associated GPLs. **E)** Open chromatin
674 tracks, split by disease (beige box – steady state; maroon box – AD-like disease) and by RAG
675 fate map ($RAG^{naïve}$ - gray, RAG^{exp} - red) for *Il13*.

676

677 **MATERIALS AND METHODS**

678 **Animal studies**

679 Wild-type (WT) C57BL/6J and WT congenic strains (CD90.1, CD45.1), *Rag1*$^{-/-}$, and *Rag2*$^{-}$
680 $^{/-}$ mice were initially purchased from the Jackson Laboratory and bred in house. The RAG fate-
681 mapping strain *Rag1*^{Cre}::*Rosa26*$^{LSL\text{-}tdRFP}$ was originally created in the lab of Paul Kincade[33] and
682 bred in house. All mice were housed in specific-pathogen-free condition and environmentally
683 controlled animal faculty with a 12-hour light-dark cycle and given unrestricted access to food and
684 water at Icahn School of Medicine at Mount Sinai or Washington University School of Medicine in
685 St. Louis. All animal protocols and experiments were approved by the Institutional Animal Care
686 and Use Committee (IACUC) at Icahn School of Medicine at Mount Sinai or Washington
687 University School of Medicine in St. Louis. Experiments were performed on independent cohorts
688 of male and female mice. For induction of AD-like disease, 8- to 12-week-old mice were treated
689 with 2 nmol calcipotriol (MC903, Tocris Bioscience) in 10 µL of 100% ethanol (EtOH) vehicle, or
690 vehicle alone, on the bilateral ear skin daily for 7-10 days. Body weight and ear thickness were
691 measured daily with a digital scale and analog caliper by the same investigator. For tissue harvest,
692 animals were euthanized by CO_2 inhalation.

693 **Flow cytometry**

694 Cervical skin draining lymph nodes (sdLN) were removed from the mice and immediately
695 homogenized manually through a 100 µm cell strainer (Fisher Scientific) into a 50 mL tube with
696 the end of a plunger from a 3 mL syringe. The strainer was washed with wash medium (2% vol/vol
697 FBS/PBS) and the strained cells were centrifuged at 400g for 5 minutes at 4°C. Lymph node cell
698 samples were stained with Zombie NIR viability dye (Biolegend; 1:500) to exclude dead cells,
699 followed by Fc-receptor blocking and cell-surface staining with specific antibodies. The cells were
700 analyzed using either LSR Fortessa™ (BD) or Cytek® Aurora (CYTEK) flow cytometers. Data was

701 obtained using either FACSDiva™ (BD) or SpectroFlo® (CYTEK) software and was further
702 analyzed using FlowJo™.

703 **Lymphocyte stimulations**

704 After tissue harvest, ILC stimulations were performed by incubating 0.5-1x10^6 cells for 4
705 hours at 37°C in stimulation media (DMEM with 5% fetal bovine serum, 1%
706 penicillin/streptomycin, 2 mM L-glutamine, 50 ng/mL Phorbol 12-myristate 13-acetate (PMA), 100
707 ng/mL ionomycin, 5 ug/mL Brefeldin A (BFA), 2 uM monensin). T cell stimulations were performed
708 by first coating a 96-well plate with 5 µg/mL anti-mouse CD3 (Biolegend) in 50 µL/well PBS
709 overnight the day before tissue harvest. The following day, 0.5-1x10^6 cells were resuspended in
710 50 µL/well T cell stimulation media (5 µg/mL anti-mouse CD28 (Biolegend), 5 ug/mL BFA), 2 µM
711 monensin) and incubated for 20 minutes hours at 37 C. The cells were then transferred to the
712 anti-mouse CD3 coated plate and incubated for 4 hours at 37 C. After stimulation, cells were
713 washed in wash medium, fixed, and stained for surface and intracellular markers as described for
714 unstimulated cells.

715 **Splenocyte chimeras**

716 Spleens were harvested from donor WT B6 mice and immediately homogenized manually
717 through a 100 µm cell strainer (Fisher Scientific) into a 50 mL tube with the end of a plunger from
718 a 3 mL syringe. The strainer was washed with wash medium (2% vol/vol FBS/PBS) and the
719 strained cells were centrifuged at 400g for 5 minutes at 4°C followed by treatment with RBC lysis
720 buffer for two minutes and two wash steps using 2 volumes of wash medium. Cells were counted,
721 and 5 million splenocytes were injected intraperitoneally into each recipient mouse. Experiments
722 were performed 4 weeks following splenocyte add-back to allow immune reconstitution.

723 **Bone marrow chimeras**

724 Recipient mice were provided with antibiotic water, consisting of 5 mL of Sulfatrim
725 (sulfamethoxazole/trimethoprim) added into 200 mL of drinking water, for one week starting from
726 the day prior to irradiation (day -1). On day 0, recipient mice were irradiated with 950 cGy using
727 the X-RAD 320 (Precision X-Ray). BM was harvested from donor mice femurs and tibias and
728 treated with RBC lysis buffer (Sigma-Aldrich) for two minutes. BM cells were transferred into a 15
729 mL conical tube through a 70 µm cell strainer (Fisher Scientific) and the cell strainer and cells
730 were washed with 2% (vol/vol) FBS/PBS. The concentration of living cells was determined using
731 a Cellometer Auto 2000 (Nexcelom Bioscience) with ViaStain™ AOPI Staining Solution
732 (Nexcelom Bioscience). Recipient mice received the same number of cells, at 1 x 10^7 live bone
733 marrow cells per mouse, through retroorbital injection within 24-hour after irradiation. Recipients
734 were given 8 weeks for immune reconstitution after BM transplantation before experimental use.

735 **Cryopreserving sdLN cells for sequencing**

736 *Rag1*^{Cre}::*Rosa26*$^{LSL\text{-}tdRFP}$ mice were treated with 2 nmol calcipotriol (MC903, Tocris
737 Bioscience) in 10 µL of 100% ethanol (EtOH) vehicle, or vehicle alone, on the bilateral ear skin
738 daily for 7 days to induce AD-like inflammation. The next day, cervical sdLN were harvested and
739 immediately homogenized manually through a 100 µm cell strainer (Fisher Scientific) into a 50
740 mL tube with the end of a plunger from a 3 mL syringe. The strainer was washed with wash
741 medium (2% vol/vol FBS/PBS) and the strained cells were centrifuged at 400g for 5 minutes at
742 4°C. Next, cells were incubated with biotinylated antibodies (anti-mouse CD3e, CD19, CD11b;
743 1:300; Biolegend) in 100 µL of wash buffer for 20 minutes at 4°C, followed by two washes in 2
744 volumes of wash buffer. Next, no more than 10^7 cells were incubated with Streptavidin
745 MicroBeads (Miltenyi) in 500 µL separation buffer (0.5% w/v BSA in PBS; BSA and PBS from
746 Sigma) at 4°C for 20 minutes, then added to LD columns (Miltenyi) pre-equilibrated with
747 separation buffer and loaded in a QuadroMACS™ Separator (Miltenyi) for negative cell selection.

748 Remaining cells were eluted in 1 mL separation buffer and cells were centrifuged at 400g for 5
749 minutes at 4°C, followed by resuspension in freezing buffer (10% DMSO, Invitrogen; 20% FBS in
750 DMEM, Sigma) and slow freezing to -80°C in a CoolCell™ LX (Corning) device.

751 **Processing cryopreserved cells for multiome**

752 Cryopreserved sdLN cells were processed as recommended by the 10X Genomics
753 DemonstratedProtocol_NucleiIsolation_ATAC_GEX_Sequencing_RevC_(CG000365)
754 instructions for primary cells without any modification to the protocol. Briefly, cells were thawed in
755 a 37°C water bath followed by dilution into media (RPMI + 15% FBS, Sigma) and centrifugation
756 at 400g for 5 minutes at 4°C. For each final sample (EtOH vehicle- or MC903-treated), cells were
757 pooled from sample from 3 individual mice. Cells were resuspended in PBS + 0.04% BSA (Sigma)
758 and passed through a 40 µm Flomi strainer (Bel-art) followed by determination of cell
759 concentration using the using Cellometer Auto 2000 (Nexcelom Bioscience) with ViaStain™ AOPI
760 Staining Solution (Nexcelom Bioscience). Cells were centrifuged 5 minutes at 4°C and
761 supernatant removed. Lysis Buffer (Tris HCl base with 0.1% Tween-20, 0.1% NP-40, 0.01%
762 digitonin, 1 mM DTT, and 1 U/µL Protectors RNase inhibitor, Sigma; full recipe in 10X protocol)
763 was added, cells mixed 10x, and incubated on ice for 3 minutes. Nuclei from lysed cells were
764 centrifuged at 400g for 5 minutes at 4°C and washed in 1 mL Wash Buffer (Lysis Buffer, but
765 without NP-40 or digitonin). The wash step was repeated two more times. Nuclei concentration
766 was determined as for cell concentration using the Cellometer and ViaStain™ solution. The AOPI
767 staining indicated 97-99% lysis efficiency of the cells. We manually confirmed nuclei count using
768 a Bright-Line™ hemacytometer (Hausser Scientific™). Nuclei were centrifuged at 400g for 5
769 minutes and resuspended in a volume of 1X Nuclei Buffer (10X Genomics) to yield roughly 4,000
770 nuclei/µL. We then immediately proceeded to the 10X Chromium Next GEM Single Cell Multiome
771 ATAC + Gene Expression pipeline.

772 **Multiome library construction and sequencing**

773 Multiome 3v3.1 GEX and ATAC libraries were prepared as recommended by 10X
774 Genomics protocol Chromium_NextGEM_Multiome_ATAC_GEX_User_Guide_RevD
775 ((CG000338). For sample preparation on the 10x Genomics platform, the Chromium Next GEM
776 Single Cell Multiome ATAC + Gene Expression Reagent Bundle, 16 rxns PN-
777 1000283, Chromium Next GEM Chip J Single Cell Kit, 48 rxns PN-1000234, Single Index Kit N
778 Set A, 96 rxns PN-1000212 (ATAC), Dual Index Kit TT Set A, 96 rxns PN-1000215 (3v3.1 GEX),
779 were used. The concentration of each library was accurately determined through qPCR utilizing
780 the KAPA library Quantification Kit according to the manufacturer's protocol (KAPA
781 Biosystems/Roche) to produce cluster counts appropriate for the Illumina NovaSeq6000
782 instrument. GEX libraries were pooled and run over 0.05 of a NovaSeq6000 S4 flow cell using
783 the XP workflow and running a 28x10x10x150 sequencing recipe in accordance with
784 manufacturer's protocol. Target coverage was 500M reads per sample. ATAC libraries were
785 pooled and run over 0.167 of a NovaSeq6000 S1 flow cell using the XP workflow and running a
786 51x8x16x51 sequencing recipe in accordance with manufacturer's protocol. Target coverage
787 was 250M reads per sample.

788 **Multiomic data analysis**

789 The cellranger-arc-2.0.0 (10X Genomics) pipeline was used to generate FASTQ files,
790 gene expression matrices, and ATAC fragment tables for each sample, followed by aggregation
791 using the aggr function. Default settings were utilized, with the exception that we incorporated a
792 custom reference with the sequence for tdRFP (see **Supplemental file S1**) added to the default
793 mouse reference sequence provided by cellranger (refdata-cellranger-arc-mm10-2020-A-2.0.0).
794 Correction for ambient RNA was performed using SoupX[123] with clustering information provided
795 by the default cellranger outputs. Doublets were removed using Scrublet[124] with default settings.

796 Corrected data was then processed using Signac[37] and Seurat[34–36]. ATAC-seq peaks were
797 identified using MACS2[125] through the CallPeaks function in Signac. Per-cell quality control
798 metrics were computed using the TSSEnrichment and NucleosomeSignal functions, and cells
799 retained with a nucleosome signal score < 1.5, TSS enrichment score > 1, total RNA counts <
800 15,000 and > 1,000, total ATAC counts < 75,000 and > 100, percent mitochondrial reads < 5%,
801 and percent ribosomal genes detected <10%. After these filtering steps, 10,304 cells remained.
802 Cells were further filtered by their expression of lineage defining markers similar to the negative
803 selection step during sample processing. Cells with detectable transcripts for *Cd3d*, *Cd3e*, *Cd3g*,
804 *Cd4*, *Cd19*, *Cd8a*, and *Itgam* were removed. This left 2,034 remaining cells for further analysis.

805 The SCTransform function of Seurat was used to normalize RNA counts. We performed
806 integration of the two samples using the RNA assay to correct for batch effects and treatment in
807 the initial clustering using the default parameters for the functions SelectIntegrationFeatures,
808 FindIntegrationAnchors, and IntegrateData. The integrated data was used for PCA (25
809 dimensions) and UMAP reduction for the RNA assay alone. With default parameters in Signac,
810 we used TFIDF to normalize ATAC peaks and latent semantic indexing (LSI) to reduce the
811 dimensionality of the ATAC data. We constructed a UMAP of the ATAC data alone using the LSI
812 reduction (dimensions 2-25). To construct a joint graph and UMAP using equal weighting from
813 the RNA and ATAC assays, we used the FindMultiModalNeighbors function of Seurat/Signac
814 using default parameters (RNA dimensions 1-25, ATAC dimensions 2-25). We used a resolution
815 of 0.1 to identify clusters with the FindClusters function in Seurat/Signac. Cell types were assigned
816 based on manual curation of marker genes. Initially, 7 clusters were identified, but two highly
817 similar lymphocyte clusters were merged for a total of 6 cell types.

818 The inferred Gene Activity (GA) assay from the ATAC-seq data was calculated using
819 default parameters of the GeneActivity function in Signac. FindAllMarkers was used to identify
820 top markers by cluster for both RNA gene expression data (GEX) and GA, with setting

821 adjustments including min.pct = 0.20 and logfc.threshold = 0.25. The differentially accessible (DA)
822 open chromatin assay was calculated in Signac with the FindMarkers function on the ATAC-seq
823 peaks assay (called using MACS2 as above). The differential test used was 'LR' (logistical
824 regression, as suggested for snRNA-seq[126]). The total number of ATAC fragments was used as
825 a latent variable to mitigate effect of differential sequencing depth. Given the sparsity of the data,
826 the min.pct parameter was set to 0.02. After identifying the top differentially accessible peaks for
827 each cluster, the gene closest to each peak was determined using the ClosestFeature function in
828 Signac. Results were filtered for genes within 10^5 base pairs of the corresponding peak. The
829 filtered gene lists were used for the "DA" assay as markers of each cluster (top 25) and an
830 expanded list for the ILC2 cluster (top 100). Venn diagrams were calculated using
831 BioVenn/BioVennR[127].

832 Gene set enrichment analysis was performed and visualized using ClusterProfiler[128]. For
833 GSEA on steady state ILC2 DEGs between fate mapped states, we opted to use more permissive
834 filtering parameters instead of default parameters. We created the ranked list of DEGs using the
835 FindMarkers function in Seurat with min.pct = 0.1 and logfc.threshold = 0.1. The DEG list from
836 the GEX assay was used to generate the GSEA results. The DEG list from the GA assay did not
837 yield any significant GSEA results. The ClusterProfiler function gseGO was used to analyze the
838 ranked DEG list using the paramters minGSSize = 50, maxGSSize = 500, pvalueCutoff = 0.05.

839 The correlation coefficients, or gene to peak links (GPLs), between gene expression and
840 accessibility of each peak were calculated for all peaks within 10^6 base pairs of the transcription
841 start sites for all detected genes using the LinkPeaks function of Signac with min.cells = 2. GPLs
842 were filtered by gene for the curated ILC2 and Th2 gene sets. Since multiple genes can be linked
843 to one peak by GPL analysis, finding intersections of GPLs in set analysis would result in counting
844 some epigenomic regions multiple times. Thus, for set analysis, we eliminated GPLs with
845 redundant peaks. Then, we used each list of non-redundant peaks as input sets to generate
846 UpSet plots and lists of intersecting peaks between states (Rag1 fate map positive or negative;

AD-like disease or steady state) using UpSetR[129]. Coverage plots of the single cell multiomic data, including open chromatin, peaks, and links (GPLs), were plotted using the CoveragePlot function in Signac.

Data and code availability

Sequencing data have been deposited at GEO and accession numbers are listed in the key resources table. Aggregated data are supplied in the supplemental file. All data reported in this paper will be shared by the lead contact upon request. This paper does not report original code. Any additional information required to reanalyze the data reported in this paper is available from the lead contact upon request.

REAGENT or RESOURCE	SOURCE	IDENTIFIER
Antibodies		
anti-mouse CD11b	eBioscience	Cat#: 45-0112-82; RRID: AB_953558
anti-mouse CD11c	eBioscience	Cat#: 45-0114-82; RRID: AB_925727
anti-mouse CD19	eBioscience	Cat#: 45-0193-82; RRID: AB_1106999
anti-mouse CD3e	eBioscience	Cat#: 45-0031-82; RRID: AB_1107000
anti-mouse CD5	eBioscience	Cat#: 45-0051-82; RRID: AB_914334
anti-mouse NK1.1	eBioscience	Cat#: 45-5941-82; RRID: AB_914361
anti-mouse FcεR1α	eBioscience	Cat#: 11-5898-82; RRID: AB_465308
anti-mouse IL-13	eBioscience	Cat#: 48-7136-42; RRID: AB_2784729
anti-mouse CD45.1	BioLegend	Cat#: 110706; RRID: AB_313495
anti-mouse CD45.2	BioLegend	Cat#: 109808; RRID: AB_313445
anti-mouse ICOS	BioLegend	Cat#: 313506; RRID: AB_416330
anti-mouse CD62L	BioLegend	Cat#: 104428; RRID: AB_830799
anti-mouse CD69	BioLegend	Cat#: 104530; RRID: AB_2563062
anti-mouse KLRG1	BioLegend	Cat#: 138424; RRID: AB_2564051
anti-mouse IL-5	BioLegend	Cat#: 504306; RRID: AB_315330
anti-mouse IL-13	BioLegend	Cat#: 503826; RRID: AB_2650897
anti-mouse IL-17A	BioLegend	Cat#: 506927; RRID: AB_11126144
anti-mouse IFNγ	BioLegend	Cat#: 505806; RRID: AB_315400
anti-mouse CD90.2	BioLegend	Cat#: 105328; RRID: AB_10613293
anti-mouse IL-33Rα	BioLegend	Cat#: 145308; RRID: AB_2565569
anti-mouse IL-33Rα	BioLegend	Cat#: 145327; RRID: AB_2565569
anti-mouse CD8a	BioLegend	Cat#: 100762; RRID: AB_2564027
anti-mouse CD25	BioLegend	Cat#: 102016; RRID: AB_312865
anti-mouse CD45.2	BioLegend	Cat#: 109806; RRID: AB_313443
anti-mouse CD90.2	BioLegend	Cat#: 109830; RRID: AB_1186098
anti-mouse CD4	BioLegend	Cat#: 100449; RRID: AB_2564587
anti-mouse Gata3	BioLegend	Cat#: 653814; RRID: AB_2563221
anti-mouse CD25	BioLegend	Cat#: 102036; RRID: AB_2563059
anti-mouse CD90.1	BioLegend	Cat#: 202537; RRID: AB_2562644
anti-mouse CD3e	BioLegend	Cat#: 155608; RRID: AB_2750434
anti-mouse CD3e	BioLegend	Cat#: 100339; RRID: AB_11150783
anti-mouse CD28	BioLegend	Cat#: 102115; RRID: AB_11150408
anti-mouse CD3	BioLegend	Cat#: 100243; RRID: AB_2563946
anti-mouse CD19	BioLegend	Cat#: 115503; RRID: AB_313638
anti-mouse CD11b	BioLegend	Cat#: 101203; RRID: AB_312786
anti-mouse IL-4	BioLegend	Cat#: 504109; RRID: AB_493320
anti-mouse CD117 (c-Kit)	BioLegend	Cat#: 105838; RRID: AB_2616739
anti-mouse CD49b	Invitrogen	Cat#: 17-5971-82; RRID: AB_469485
anti-mouse CD45R/B220	BioLegend	Cat#: 103275; RRID: AB_2860602
anti-mouse I-A/I-E (MHCII)	BioLegend	Cat#: 107622; RRID: AB_493727
anti-mouse Ly-6A/E (Sca-1)	BioLegend	Cat#: 122512; RRID: AB_756197
anti-mouse F4/80	BioLegend	Cat#: 123112; RRID: AB_893482

anti-mouse SiglecF	BD Biosciences	Cat#: 562757; RRID: AB_2687994
anti-mouse TCR γ/δ	eBioscience	Cat#: 48-5711-82; RRID: AB_2574071
anti-mouse Ly-6G	eBioscience	Cat#: 62-9668-82; RRID: AB_2762763
anti-mouse CD16/CD32	Bio X Cell	Cat#: BE0307; RRID: AB_1107647
streptavidin	BioLegend	Cat#: 405204
streptavidin	BioLegend	Cat#: 405207
Chemicals, peptides, and recombinant proteins		
Phorbol 12-myristate 13-acetate (PMA)	Sigma	P1585
Ionomycin	Sigma	I0634
Monensin	Biolegend	420701
Brefeldin A Solution	Biolegend	420601
DMEM	Sigma	D6429
RPMI-1640 Medium	Sigma	R8758
Bovine serum albumin (BSA)	Sigma	A2058
Penicillin-Streptomycin	Gibco	15140122
L-glutamine solution - 200 mM	Corning	MT25005CI
Fetal bovine serum	Sigma	2442
Calcipotriol (MC903)	Tocris Biosciences	2700
Phosphate Buffered Saline	Sigma	806552
DMSO	Invitrogen	D12345
Nuclei Buffer (20X)	10x Genomics	2000153/2000207
Digitonin	ThermoFisher	BN2006
Trizma hydrochloride solution pH 7.4	Sigma	T2194
Sodium Chloride Solution 5 M	Sigma	59222C
Magnesium Chloride Solution 1M	Sigma	M1028
Nonidet P40 Substitute	Sigma	74385
Protector RNase inhibitor	Sigma	3335402001
DTT	Sigma	646563
Flowmi Cell Strainer 40 µm	Bel-Art	H13680-0040
Tween 20	Bio-Rad	1662404
ZombieNIR	Biolegend	423106
ZombieUV	Biolegend	423107
Experimental models: Organisms/strains		
B6 WT	Jackson Laboratory	C57BL/6J; Cat# 000664
Rag1$^{-/-}$	Jackson Laboratory	B6.129S7-Rag1tm1Mom/J; Cat# 002216
Rag2$^{-/-}$	Jackson Laboratory	B6.Cg-Rag2tm1.1Cgn/J; Cat# 002014
B6 CD45.1	Jackson Laboratory	B6.SJL-Ptprca Pepcb/BoyJ; Cat# 008450
B6 CD90.1	Jackson Laboratory	B6.PL-Thy1a/CyJ; Cat# 000406
Rag1 fate-map mice	[24,33]	

Software and algorithms		
BD FACSDiva (v8.0)	BD Life Sciences	https://www.bdbiosciences.com/en-us/products/software/instrument-software/bd-facsdiva-software
FlowJo™ (v10.8)	BD Life Sciences	https://www.flowjo.com/
SpectroFlo® (v3.0)	CYTEK	https://cytekbio.com/pages/spectro-flo
Prism 9	GraphPad Software	https://www.graphpad.com/scientific-software/prism/
R (v4.2.2)	R core	https://www.r-project.org/
Seurat (v4.2.0)	[35]	https://github.com/satijalab/seurat
Signac (v1.8.0)	[37]	https://github.com/stuart-lab/signac
chromVAR (v1.18.0)	[130]	https://github.com/GreenleafLab/chromVAR
JASPAR2022 (v0.99.7)		https://github.com/da-bar/JASPAR2022
SoupX (v1.6.1)	[123]	https://github.com/constantAmateur/SoupX
clusterProfiler (v4.4.4)	[128]	https://github.com/YuLab-SMU/clusterProfiler
singleCellTK (v2.6.0)	[131]	https://github.com/compbiomed/singleCellTK
biomaRt (v2.52.0)	[132]	https://github.com/grimbough/biomaRt
EnsDb.Mmusculus.v79 (v2.99.0)	[133]	https://bioconductor.org/packages/release/data/annotation/html/EnsDb.Mmusculus.v79.html
BSgenome.Mmusculus.UCSC.mm10 (v1.4.3)	[134]	https://bioconductor.org/packages/release/data/annotation/html/BSgenome.Mmusculus.UCSC.mm10.html
ggplot2 (v3.3.6)	[135]	https://github.com/tidyverse/ggplot2
viridis (v0.6.2)	[136]	https://github.com/sjmgarnier/viridis
TFBSTools (v1.34.0)	[137]	https://bioconductor.org/packages/release/bioc/html/TFBSTools.html
motifmatchr (v1.18.0)	[138]	https://github.com/GreenleafLab/motifmatchr
BioVenn/BioVennR	[127]	https://www.biovenn.nl/
UpSetR	[129]	http://gehlenborglab.org/research/projects/upsetr/
Cell Ranger	[139,140]	https://support.10xgenomics.com/single-cell-multiome-atac-gex/software/overview/welcome
Python (v3.7)	Python Software Foundation	https://www.python.org/
Deposited data		
scRNA-seq dataset	This paper	GEO: GSE192597

scATAC-seq dataset	This paper	GEO: GSE192597
Other		
Streptavidin MicroBeads	Miltenyi	130-048-101
LD Columns	Miltenyi	130-042-901
QuadroMACS™ Separator	Miltenyi	130-090-976
CoolCell™ LX	Corning	CLS432001
Bright-Line™ hemacytometer	Hausser Scientific	3110V
Cytek® Aurora	CYTEK	N/A
LSR FortessaTM	BD Life Sciences	N/A

858

859 **REFERENCES**
860

861 1. Ständer, S. Atopic Dermatitis. *New Engl J Med* **384,** 1136–1143 (2021).

862 2. Hammad, H. & Lambrecht, B. N. The basic immunology of asthma. *Cell* **184,** 1469–1485
863 (2021).

864 3. Yu, W., Freeland, D. M. H. & Nadeau, K. C. Food allergy: immune mechanisms, diagnosis
865 and immunotherapy. *Nat Rev Immunol* **16,** 751–765 (2016).

866 4. Tordesillas, L., Berin, M. C. & Sampson, H. A. Immunology of Food Allergy. *Immunity* **47,** 32–
867 50 (2017).

868 5. Ring, J. Terminology of Allergic Phenomena. *Chem Immunol Allergy* **100,** 46–52 (2014).

869 6. Halim, T. Y. F., Hwang, Y. Y., Scanlon, S. T., Zaghouani, H., Garbi, N., Fallon, P. G. &
870 McKenzie, A. N. J. Group 2 innate lymphoid cells license dendritic cells to potentiate memory
871 TH2 cell responses. *Nat Immunol* **17,** 57–64 (2016).

872 7. Halim, T. Y. F., Steer, C. A., Mathä, L., Gold, M. J., Martinez-Gonzalez, I., McNagny, K. M.,
873 McKenzie, A. N. J. & Takei, F. Group 2 Innate Lymphoid Cells Are Critical for the Initiation of
874 Adaptive T Helper 2 Cell-Mediated Allergic Lung Inflammation. *Immunity* **40,** 425–435 (2014).

875 8. Sokol, C. L., Chu, N.-Q., Yu, S., Nish, S. A., Laufer, T. M. & Medzhitov, R. Basophils function
876 as antigen-presenting cells for an allergen-induced T helper type 2 response. *Nat. Immunol.* **10,**
877 713–720 (2009).

878 9. Perrigoue, J. G., Saenz, S. A., Siracusa, M. C., Allenspach, E. J., Taylor, B. C., Giacomin, P.
879 R., Nair, M. G., Du, Y., Zaph, C., Rooijen, N. van, Comeau, M. R., Pearce, E. J., Laufer, T. M. &
880 Artis, D. MHC class II–dependent basophil–CD4+ T cell interactions promote TH2 cytokine–
881 dependent immunity. *Nat Immunol* **10,** 697–705 (2009).

882 10. Vivier, E., Artis, D., Colonna, M., Diefenbach, A., Santo, J. P. D., Eberl, G., Koyasu, S.,
883 Locksley, R. M., McKenzie, A. N. J., Mebius, R. E., Powrie, F. & Spits, H. Innate Lymphoid
884 Cells: 10 Years On. *Cell* **174,** 1054–1066 (2018).

885 11. Imai, Y., Yasuda, K., Sakaguchi, Y., Haneda, T., Mizutani, H., Yoshimoto, T., Nakanishi, K.
886 & Yamanishi, K. Skin-specific expression of IL-33 activates group 2 innate lymphoid cells and
887 elicits atopic dermatitis-like inflammation in mice. *P Natl Acad Sci Usa* **110,** 13921–6 (2013).

888 12. Salimi, M., Barlow, J. L., Saunders, S. P., Xue, L., Gutowska-Owsiak, D., Wang, X., Huang,
889 L.-C., Johnson, D., Scanlon, S. T., McKenzie, A. N. J., Fallon, P. G. & Ogg, G. S. A role for IL-
890 25 and IL-33–driven type-2 innate lymphoid cells in atopic dermatitis. *J Exp Med* **210,** 2939–
891 2950 (2013).

892 13. Kim, B. S., Siracusa, M. C., Saenz, S. A., Noti, M., Monticelli, L. A., Sonnenberg, G. F.,
893 Hepworth, M. R., Voorhees, A. S. V., Comeau, M. R. & Artis, D. TSLP elicits IL-33-independent
894 innate lymphoid cell responses to promote skin inflammation. *Sci Transl Med* **5,** 170ra16 (2013).

895 14. Tsou, A. M., Yano, H., Parkhurst, C. N., Mahlakõiv, T., Chu, C., Zhang, W., He, Z., Jarick, K.
896 J., Zhong, C., Putzel, G. G., Hatazaki, M., Consortium, J. I. L. C. B., Longman, R., Sonnenberg,
897 G., Scherl, E., Lukin, D., Battat, R., Sockolow, R., Ciecierega, T., Solomon, A., Barfield, E.,
898 Chien, K., Ferreira, J., Williams, J., Khan, S., Chong, P. S., Mozumder, S., Chou, L., Zhou, W.,
899 Ahmed, A., Joseph, A. M., Lorenz, I. C., Andrew, D., Balderes, P., Klose, C. S. N., Lira, S. A. &
900 Artis, D. Neuropeptide regulation of non-redundant ILC2 responses at barrier surfaces. *Nature*
901 **611,** 787–793 (2022).

902 15. Jarick, K. J., Topczewska, P. M., Jakob, M. O., Yano, H., Arifuzzaman, M., Gao, X.,
903 Boulekou, S., Stokic-Trtica, V., Leclère, P. S., Preußer, A., Rompe, Z. A., Stamm, A., Tsou, A.
904 M., Chu, C., Heinrich, F. R., Guerra, G. M., Durek, P., Ivanov, A., Beule, D., Helfrich, S., Duerr,
905 C. U., Kühl, A. A., Stehle, C., Romagnani, C., Mashreghi, M.-F., Diefenbach, A., Artis, D. &
906 Klose, C. S. N. Non-redundant functions of group 2 innate lymphoid cells. *Nature* **611,** 794–800
907 (2022).

908 16. Fort, M. M., Cheung, J., Yen, D., Li, J., Zurawski, S. M., Lo, S., Menon, S., Clifford, T.,
909 Hunte, B., Lesley, R., Muchamuel, T., Hurst, S. D., Zurawski, G., Leach, M. W., Gorman, D. M.
910 & Rennick, D. M. IL-25 Induces IL-4, IL-5, and IL-13 and Th2-Associated Pathologies In Vivo.
911 *Immunity* **15,** 985–995 (2001).

912 17. Hurst, S. D., Muchamuel, T., Gorman, D. M., Gilbert, J. M., Clifford, T., Kwan, S., Menon, S.,
913 Seymour, B., Jackson, C., Kung, T. T., Brieland, J. K., Zurawski, S. M., Chapman, R. W.,
914 Zurawski, G. & Coffman, R. L. New IL-17 Family Members Promote Th1 or Th2 Responses in
915 the Lung: In Vivo Function of the Novel Cytokine IL-25. *J Immunol* **169,** 443–453 (2002).

916 18. Fallon, P. G., Ballantyne, S. J., Mangan, N. E., Barlow, J. L., Dasvarma, A., Hewett, D. R.,
917 McIlgorm, A., Jolin, H. E. & McKenzie, A. N. J. Identification of an interleukin (IL)-25–dependent
918 cell population that provides IL-4, IL-5, and IL-13 at the onset of helminth expulsion. *J Exp*
919 *Medicine* **203,** 1105–1116 (2006).

920 19. Moro, K., Yamada, T., Tanabe, M., Takeuchi, T., Ikawa, T., Kawamoto, H., Furusawa, J.,
921 Ohtani, M., Fujii, H. & Koyasu, S. Innate production of TH2 cytokines by adipose tissue-
922 associated c-Kit+Sca-1+ lymphoid cells. *Nature* **463,** 540–544 (2010).

923 20. Saenz, S. A., Siracusa, M. C., Perrigoue, J. G., Spencer, S. P., Jr, J. F. U., Tocker, J. E.,
924 Budelsky, A. L., Kleinschek, M. A., Kastelein, R. A., Kambayashi, T., Bhandoola, A. & Artis, D.
925 IL25 elicits a multipotent progenitor cell population that promotes TH2 cytokine responses.
926 *Nature* **464,** 1362–1366 (2010).

927 21. Neill, D. R., Wong, S. H., Bellosi, A., Flynn, R. J., Daly, M., Langford, T. K. A., Bucks, C.,
928 Kane, C. M., Fallon, P. G., Pannell, R., Jolin, H. E. & McKenzie, A. N. J. Nuocytes represent a
929 new innate effector leukocyte that mediates type-2 immunity. *Nature* **464,** 1367–1370 (2010).

930 22. Price, A. E., Liang, H.-E., Sullivan, B. M., Reinhardt, R. L., Eisley, C. J., Erle, D. J. &
931 Locksley, R. M. Systemically dispersed innate IL-13-expressing cells in type 2 immunity. *P Natl*
932 *Acad Sci Usa* **107,** 11489–94 (2010).

933 23. Yang, Q., Saenz, S. A., Zlotoff, D. A., Artis, D. & Bhandoola, A. Cutting Edge: Natural Helper
934 Cells Derive from Lymphoid Progenitors. *J Immunol* **187,** 5505–5509 (2011).

935 24. Karo, J. M., Schatz, D. G. & Sun, J. C. The RAG Recombinase Dictates Functional
936 Heterogeneity and Cellular Fitness in Natural Killer Cells. *Cell* **159,** 94–107 (2014).

937 25. Bredemeyer, A. L., Helmink, B. A., Innes, C. L., Calderon, B., McGinnis, L. M., Mahowald,
938 G. K., Gapud, E. J., Walker, L. M., Collins, J. B., Weaver, B. K., Mandik-Nayak, L., Schreiber, R.
939 D., Allen, P. M., May, M. J., Paules, R. S., Bassing, C. H. & Sleckman, B. P. DNA double-strand
940 breaks activate a multi-functional genetic program in developing lymphocytes. *Nature* **456,** 819–
941 823 (2008).

942 26. Bednarski, J. J., Nickless, A., Bhattacharya, D., Amin, R. H., Schlissel, M. S. & Sleckman, B.
943 P. RAG-induced DNA double-strand breaks signal through Pim2 to promote pre–B cell survival
944 and limit proliferation. *J. Exp. Med.* **209,** 11–17 (2012).

945 27. Teng, G., Maman, Y., Resch, W., Kim, M., Yamane, A., Qian, J., Kieffer-Kwon, K.-R.,
946 Mandal, M., Ji, Y., Meffre, E., Clark, M. R., Cowell, L. G., Casellas, R. & Schatz, D. G. RAG
947 Represents a Widespread Threat to the Lymphocyte Genome. *Cell* **162,** 751–765 (2015).

948 28. Li, M., Hener, P., Zhang, Z., Kato, S., Metzger, D. & Chambon, P. Topical vitamin D3 and
949 low-calcemic analogs induce thymic stromal lymphopoietin in mouse keratinocytes and trigger
950 an atopic dermatitis. *Proc National Acad Sci* **103,** 11736–11741 (2006).

951 29. Liu, C., Zhang, Y., Liu, C. C. & Schatz, D. G. Structural insights into the evolution of the
952 RAG recombinase. *Nat Rev Immunol* 1–18 (2021). doi:10.1038/s41577-021-00628-6

953 30. Shih, H.-Y., Sciumè, G., Mikami, Y., Guo, L., Sun, H.-W., Brooks, S. R., Urban, J. F., Davis,
954 F. P., Kanno, Y. & O'Shea, J. J. Developmental Acquisition of Regulomes Underlies Innate
955 Lymphoid Cell Functionality. *Cell* **165,** 1120–1133 (2016).

956 31. Dyken, S. J. V., Nussbaum, J. C., Lee, J., Molofsky, A. B., Liang, H.-E., Pollack, J. L., Gate,
957 R. E., Haliburton, G. E., Ye, C. J., Marson, A., Erle, D. J. & Locksley, R. M. A tissue checkpoint
958 regulates type 2 immunity. *Nat Immunol* **17,** 1381–1387 (2016).

959 32. Turka, L. A., Schatz, D. G., Oettinger, M. A., Chun, J. J. M., Gorka, C., Lee, K., McCormack,
960 W. T. & Thompson, C. B. Thymocyte Expression of RAG-1 and RAG-2: Termination by T Cell
961 Receptor Cross-Linking. *Science* **253,** 778–781 (1991).

962 33. Welner, R. S., Esplin, B. L., Garrett, K. P., Pelayo, R., Luche, H., Fehling, H. J. & Kincade,
963 P. W. Asynchronous RAG-1 Expression during B Lymphopoiesis. *J Immunol* **183,** 7768–7777
964 (2009).

965 34. Stuart, T., Butler, A., Hoffman, P., Hafemeister, C., Papalexi, E., Mauck, W. M., Hao, Y.,
966 Stoeckius, M., Smibert, P. & Satija, R. Comprehensive Integration of Single-Cell Data. *Cell* **177,**
967 1888-1902.e21 (2019).

968 35. Hao, Y., Hao, S., Andersen-Nissen, E., Mauck, W. M., Zheng, S., Butler, A., Lee, M. J., Wilk,
969 A. J., Darby, C., Zager, M., Hoffman, P., Stoeckius, M., Papalexi, E., Mimitou, E. P., Jain, J.,
970 Srivastava, A., Stuart, T., Fleming, L. M., Yeung, B., Rogers, A. J., McElrath, J. M., Blish, C. A.,
971 Gottardo, R., Smibert, P. & Satija, R. Integrated analysis of multimodal single-cell data. *Cell*
972 (2021). doi:10.1016/j.cell.2021.04.048

973 36. Butler, A., Hoffman, P., Smibert, P., Papalexi, E. & Satija, R. Integrating single-cell
974 transcriptomic data across different conditions, technologies, and species. *Nat Biotechnol* **36,**
975 411–420 (2018).

976 37. Stuart, T., Srivastava, A., Madad, S., Lareau, C. A. & Satija, R. Single-cell chromatin state
977 analysis with Signac. *Nat Methods* **18,** 1333–1341 (2021).

978 38. Ghaedi, M., Shen, Z. Y., Orangi, M., Martinez-Gonzalez, I., Wei, L., Lu, X., Das, A., Heravi-
979 Moussavi, A., Marra, M. A., Bhandoola, A. & Takei, F. Single-cell analysis of RORα tracer
980 mouse lung reveals ILC progenitors and effector ILC2 subsets. *J Exp Med* **217,** e20182293
981 (2019).

982 39. Maazi, H., Patel, N., Sankaranarayanan, I., Suzuki, Y., Rigas, D., Soroosh, P., Freeman, G.
983 J., Sharpe, A. H. & Akbari, O. ICOS:ICOS-Ligand Interaction Is Required for Type 2 Innate
984 Lymphoid Cell Function, Homeostasis, and Induction of Airway Hyperreactivity. *Immunity* **42,**
985 538–551 (2015).

986 40. Paclik, D., Stehle, C., Lahmann, A., Hutloff, A. & Romagnani, C. ICOS regulates the pool of
987 group 2 innate lymphoid cells under homeostatic and inflammatory conditions in mice. *Eur J*
988 *Immunol* **45,** 2766–2772 (2015).

989 41. Roediger, B., Kyle, R., Yip, K. H., Sumaria, N., Guy, T. V., Kim, B. S., Mitchell, A. J., Tay, S.
990 S., Jain, R., Forbes-Blom, E., Chen, X., Tong, P. L., Bolton, H. A., Artis, D., Paul, W. E., Groth,
991 B. F. de S., Grimbaldeston, M. A., Gros, G. L. & Weninger, W. Cutaneous immunosurveillance
992 and regulation of inflammation by group 2 innate lymphoid cells. *Nat Immunol* **14,** 564–573
993 (2013).

994 42. Roediger, B., Kyle, R., Tay, S. S., Mitchell, A. J., Bolton, H. A., Guy, T. V., Tan, S.-Y.,
995 Forbes-Blom, E., Tong, P. L., Köller, Y., Shklovskaya, E., Iwashima, M., McCoy, K. D., Gros, G.
996 L., Groth, B. F. de S. & Weninger, W. IL-2 is a critical regulator of group 2 innate lymphoid cell
997 function during pulmonary inflammation. *J Allergy Clin Immun* **136,** 1653-1663.e7 (2015).

998 43. Zeis, P., Lian, M., Fan, X., Herman, J. S., Hernandez, D. C., Gentek, R., Elias, S.,
999 Symowski, C., Knöpper, K., Peltokangas, N., Friedrich, C., Doucet-Ladeveze, R., Kabat, A. M.,
1000 Locksley, R. M., Voehringer, D., Bajenoff, M., Rudensky, A. Y., Romagnani, C., Grün, D. &
1001 Gasteiger, G. In Situ Maturation and Tissue Adaptation of Type 2 Innate Lymphoid Cell
1002 Progenitors. *Immunity* **53,** 775-792.e9 (2020).

1003 44. Ricardo-Gonzalez, R. R., Dyken, S. J. V., Schneider, C., Lee, J., Nussbaum, J. C., Liang,
1004 H.-E., Vaka, D., Eckalbar, W. L., Molofsky, A. B., Erle, D. J. & Locksley, R. M. Tissue signals
1005 imprint ILC2 identity with anticipatory function. *Nat Immunol* **19,** 1093–1099 (2018).

1006 45. Cardoso, V., Chesne, J., Ribeiro, H., Garcia-Cassani, B., Carvalho, T., Bouchery, T., Shah,
1007 K., Barbosa-Morais, N. L., Harris, N. & Veiga-Fernandes, H. Neuronal regulation of type 2
1008 innate lymphoid cells via neuromedin U. *Nature* **549,** 277–281 (2014).

1009 46. Klose, C. S. N., Mahlakõiv, T., Moeller, J. B., Rankin, L. C., Flamar, A.-L., Kabata, H.,
1010 Monticelli, L. A., Moriyama, S., Putzel, G. G., Rakhilin, N., Shen, X., Kostenis, E., König, G. M.,
1011 Senda, T., Carpenter, D., Farber, D. L. & Artis, D. The neuropeptide neuromedin U stimulates
1012 innate lymphoid cells and type 2 inflammation. *Nature* **549,** 282–286 (2017).

1013 47. Wallrapp, A., Riesenfeld, S. J., Burkett, P. R., Abdulnour, R.-E. E., Nyman, J., Dionne, D.,
1014 Hofree, M., Cuoco, M. S., Rodman, C., Farouq, D., Haas, B. J., Tickle, T. L., Trombetta, J. J.,
1015 Baral, P., Klose, C. S. N., Mahlakõiv, T., Artis, D., Rozenblatt-Rosen, O., Chiu, I. M., Levy, B.
1016 D., Kowalczyk, M. S., Regev, A. & Kuchroo, V. K. The neuropeptide NMU amplifies ILC2-driven
1017 allergic lung inflammation. *Nature* **549,** 351–356 (2017).

1018 48. Mjösberg, J. M., Trifari, S., Crellin, N. K., Peters, C. P., Drunen, C. M. van, Piet, B.,
1019 Fokkens, W. J., Cupedo, T. & Spits, H. Human IL-25- and IL-33-responsive type 2 innate
1020 lymphoid cells are defined by expression of CRTH2 and CD161. *Nat Immunol* **12,** 1055–1062
1021 (2011).

1022 49. Hung, L.-Y., Lewkowich, I. P., Dawson, L. A., Downey, J., Yang, Y., Smith, D. E. & Herbert,
1023 D. R. IL-33 drives biphasic IL-13 production for noncanonical Type 2 immunity against
1024 hookworms. *Proc National Acad Sci* **110,** 282–287 (2013).

1025 50. Mjösberg, J., Bernink, J., Golebski, K., Karrich, J. J., Peters, C. P., Blom, B., te Velde, A. A.,
1026 Fokkens, W. J., van Drunen, C. M. & Spits, H. The Transcription Factor GATA3 Is Essential for
1027 the Function of Human Type 2 Innate Lymphoid Cells. *Immunity* **37,** 649–659 (2012).

1028 51. Hoyler, T., Klose, C. S. N., Souabni, A., Turqueti-Neves, A., Pfeifer, D., Rawlins, E. L.,
1029 Voehringer, D., Busslinger, M. & Diefenbach, A. The Transcription Factor GATA-3 Controls Cell
1030 Fate and Maintenance of Type 2 Innate Lymphoid Cells. *Immunity* **37,** 634–648 (2012).

1031 52. Wolterink, R. G. J. K., Serafini, N., Nimwegen, M. van, Vosshenrich, C. A. J., Bruijn, M. J.
1032 W. de, Pereira, D. F., Fernandes, H. V., Hendriks, R. W. & Santo, J. P. D. Essential, dose-
1033 dependent role for the transcription factor Gata3 in the development of IL-5+ and IL-13+ type 2
1034 innate lymphoid cells. *Proc National Acad Sci* **110,** 10240–10245 (2013).

1035 53. Pokrovskii, M., Hall, J. A., Ochayon, D. E., Yi, R., Chaimowitz, N. S., Seelamneni, H.,
1036 Carriero, N., Watters, A., Waggoner, S. N., Littman, D. R., Bonneau, R. & Miraldi, E. R.
1037 Characterization of Transcriptional Regulatory Networks that Promote and Restrict Identities
1038 and Functions of Intestinal Innate Lymphoid Cells. *Immunity* **51,** 185-197.e6 (2019).

1039 54. Califano, D., Cho, J. J., Uddin, M. N., Lorentsen, K. J., Yang, Q., Bhandoola, A., Li, H. &
1040 Avram, D. Transcription Factor Bcl11b Controls Identity and Function of Mature Type 2 Innate
1041 Lymphoid Cells. *Immunity* **43,** 354–368 (2015).

1042 55. Walker, J. A., Oliphant, C. J., Englezakis, A., Yu, Y., Clare, S., Rodewald, H.-R., Belz, G.,
1043 Liu, P., Fallon, P. G. & McKenzie, A. N. J. Bcl11b is essential for group 2 innate lymphoid cell
1044 development. *J Exp Med* **212,** 875–882 (2015).

1045 56. Yu, Y., Wang, C., Clare, S., Wang, J., Lee, S.-C., Brandt, C., Burke, S., Lu, L., He, D.,
1046 Jenkins, N. A., Copeland, N. G., Dougan, G. & Liu, P. The transcription factor Bcl11b is
1047 specifically expressed in group 2 innate lymphoid cells and is essential for their development. *J*
1048 *Exp Med* **212,** 865–874 (2015).

1049 57. Hosokawa, H., Romero-Wolf, M., Yang, Q., Motomura, Y., Levanon, D., Groner, Y., Moro,
1050 K., Tanaka, T. & Rothenberg, E. V. Cell type–specific actions of Bcl11b in early T-lineage and
1051 group 2 innate lymphoid cells. *J Exp Med* **217,** e20190972 (2019).

1052 58. Björklund, Å. K., Forkel, M., Picelli, S., Konya, V., Theorell, J., Friberg, D., Sandberg, R. &
1053 Mjösberg, J. The heterogeneity of human CD127+ innate lymphoid cells revealed by single-cell
1054 RNA sequencing. *Nat Immunol* **17,** 451–460 (2016).

1055 59. Trabanelli, S., Ercolano, G., Wyss, T., Gomez-Cadena, A., Falquet, M., Cropp, D., Imbratta,
1056 C., Leblond, M. M., Salvestrini, V., Curti, A., Adotevi, O., Jandus, C. & Verdeil, G. c-Maf
1057 enforces cytokine production and promotes memory-like responses in mouse and human type 2
1058 innate lymphoid cells. *Embo J* **41,** e109300 (2022).

1059 60. Zook, E. C., Ramirez, K., Guo, X., Voort, G. van der, Sigvardsson, M., Svensson, E. C., Fu,
1060 Y.-X. & Kee, B. L. The ETS1 transcription factor is required for the development and cytokine-
1061 induced expansion of ILC2. *J Exp Med* **213,** 687–696 (2016).

1062 61. Wong, S. H., Walker, J. A., Jolin, H. E., Drynan, L. F., Hams, E., Camelo, A., Barlow, J. L.,
1063 Neill, D. R., Panova, V., Koch, U., Radtke, F., Hardman, C. S., Hwang, Y. Y., Fallon, P. G. &
1064 McKenzie, A. N. J. Transcription factor RORα is critical for nuocyte development. *Nat Immunol*
1065 **13,** 229–236 (2012).

1066 62. Halim, T. Y. F., MacLaren, A., Romanish, M. T., Gold, M. J., McNagny, K. M. & Takei, F.
1067 Retinoic-Acid-Receptor-Related Orphan Nuclear Receptor Alpha Is Required for Natural Helper
1068 Cell Development and Allergic Inflammation. *Immunity* **37,** 463–474 (2012).

1069 63. Ferreira, A. C. F., Szeto, A. C. H., Heycock, M. W. D., Clark, P. A., Walker, J. A., Crisp, A.,
1070 Barlow, J. L., Kitching, S., Lim, A., Gogoi, M., Berks, R., Daly, M., Jolin, H. E. & McKenzie, A. N.
1071 J. RORα is a critical checkpoint for T cell and ILC2 commitment in the embryonic thymus. *Nat*
1072 *Immunol* **22,** 166–178 (2021).

1073 64. Miyajima, Y., Ealey, K. N., Motomura, Y., Mochizuki, M., Takeno, N., Yanagita, M.,
1074 Economides, A. N., Nakayama, M., Koseki, H. & Moro, K. Effects of BMP7 produced by group 2
1075 innate lymphoid cells on adipogenesis. *Int Immunol* **32,** 407–419 (2020).

1076 65. Chen, W.-Y., Wu, Y.-H., Tsai, T.-H., Li, R.-F., Lai, A. C.-Y., Li, L.-C., Yang, J.-L. & Chang,
1077 Y.-J. Group 2 innate lymphoid cells contribute to IL-33-mediated alleviation of cardiac fibrosis.
1078 *Theranostics* **11,** 2594–2611 (2021).

1079 66. Xu, H., Ding, J., Porter, C. B. M., Wallrapp, A., Tabaka, M., Ma, S., Fu, S., Guo, X.,
1080 Riesenfeld, S. J., Su, C., Dionne, D., Nguyen, L. T., Lefkovith, A., Ashenberg, O., Burkett, P. R.,
1081 Shi, H. N., Rozenblatt-Rosen, O., Graham, D. B., Kuchroo, V. K., Regev, A. & Xavier, R. J.
1082 Transcriptional Atlas of Intestinal Immune Cells Reveals that Neuropeptide α-CGRP Modulates
1083 Group 2 Innate Lymphoid Cell Responses. *Immunity* **51,** 696-708.e9 (2019).

1084 67. Vivier, E., Pavert, S. A. van de, Cooper, M. D. & Belz, G. T. The evolution of innate lymphoid
1085 cells. *Nat Immunol* **17,** 790–794 (2016).

1086 68. Schneider, C., Lee, J., Koga, S., Ricardo-Gonzalez, R. R., Nussbaum, J. C., Smith, L. K.,
1087 Villeda, S. A., Liang, H.-E. & Locksley, R. M. Tissue-Resident Group 2 Innate Lymphoid Cells
1088 Differentiate by Layered Ontogeny and In Situ Perinatal Priming. *Immunity* **50,** 1425-1438.e5
1089 (2019).

1090 69. Bielecki, P., Riesenfeld, S. J., Hütter, J.-C., Triglia, E. T., Kowalczyk, M. S., Ricardo-
1091 Gonzalez, R. R., Lian, M., Vesely, M. C. A., Kroehling, L., Xu, H., Slyper, M., Muus, C., Ludwig,
1092 L. S., Christian, E., Tao, L., Kedaigle, A. J., Steach, H. R., York, A. G., Skadow, M. H.,
1093 Yaghoubi, P., Dionne, D., Jarret, A., McGee, H. M., Porter, C. B. M., Licona-Limón, P., Bailis,
1094 W., Jackson, R., Gagliani, N., Gasteiger, G., Locksley, R. M., Regev, A. & Flavell, R. A. Skin-
1095 resident innate lymphoid cells converge on a pathogenic effector state. *Nature* **592,** 128–132
1096 (2021).

1097 70. Sun, Z., Han, S., Zhu, X., Sato, A. & Islam, S. A. CCR8 Signaling Regulates Skin ILC2s to
1098 Promote Chronic Atopic Dermatitis. *Ssrn Electron J* (2022). doi:10.2139/ssrn.4135728

1099 71. Knipfer, L., Schulz-Kuhnt, A., Kindermann, M., Greif, V., Symowski, C., Voehringer, D.,
1100 Neurath, M. F., Atreya, I. & Wirtz, S. A CCL1/CCR8-dependent feed-forward mechanism drives
1101 ILC2 functions in type 2–mediated inflammation. *J Exp Med* **216,** 2763–2777 (2019).

1102 72. Subramanian, A., Tamayo, P., Mootha, V. K., Mukherjee, S., Ebert, B. L., Gillette, M. A.,
1103 Paulovich, A., Pomeroy, S. L., Golub, T. R., Lander, E. S. & Mesirov, J. P. Gene set enrichment
1104 analysis: A knowledge-based approach for interpreting genome-wide expression profiles. *Proc*
1105 *National Acad Sci* **102,** 15545–15550 (2005).

1106 73. Mootha, V. K., Lindgren, C. M., Eriksson, K.-F., Subramanian, A., Sihag, S., Lehar, J.,
1107 Puigserver, P., Carlsson, E., Ridderstråle, M., Laurila, E., Houstis, N., Daly, M. J., Patterson, N.,
1108 Mesirov, J. P., Golub, T. R., Tamayo, P., Spiegelman, B., Lander, E. S., Hirschhorn, J. N.,
1109 Altshuler, D. & Groop, L. C. PGC-1α-responsive genes involved in oxidative phosphorylation are
1110 coordinately downregulated in human diabetes. *Nat Genet* **34,** 267–273 (2003).

1111 74. Ma, S., Zhang, B., LaFave, L. M., Earl, A. S., Chiang, Z., Hu, Y., Ding, J., Brack, A., Kartha,
1112 V. K., Tay, T., Law, T., Lareau, C., Hsu, Y.-C., Regev, A. & Buenrostro, J. D. Chromatin
1113 Potential Identified by Shared Single-Cell Profiling of RNA and Chromatin. *Cell* **183,** 1103-
1114 1116.e20 (2020).

1115 75. Constantinides, M. G., McDonald, B. D., Verhoef, P. A. & Bendelac, A. A committed
1116 precursor to innate lymphoid cells. *Nature* **508,** 397–401 (2014).

1117 76. Seehus, C. R., Aliahmad, P., Torre, B. de la, Iliev, I. D., Spurka, L., Funari, V. A. & Kaye, J.
1118 Innate lymphoid cell development requires TOX-dependent generation of a common ILC
1119 progenitor. *Nat Immunol* **16,** 599–608 (2015).

1120 77. Aliahmad, P., Torre, B. de la & Kaye, J. Shared dependence on the DNA-binding factor TOX
1121 for the development of lymphoid tissue–inducer cell and NK cell lineages. *Nat Immunol* **11,** 945–
1122 952 (2010).

1123 78. Aliahmad, P. & Kaye, J. Development of all CD4 T lineages requires nuclear factor TOX. *J*
1124 *Exp Medicine* **205,** 245–256 (2008).

1125 79. Kasal, D. N., Liang, Z., Hollinger, M. K., O'Leary, C. Y., Lisicka, W., Sperling, A. I. &
1126 Bendelac, A. A Gata3 enhancer necessary for ILC2 development and function. *Proc National*
1127 *Acad Sci* **118,** e2106311118 (2021).

1128 80. Wei, L., Vahedi, G., Sun, H.-W., Watford, W. T., Takatori, H., Ramos, H. L., Takahashi, H.,
1129 Liang, J., Gutierrez-Cruz, G., Zang, C., Peng, W., O'Shea, J. J. & Kanno, Y. Discrete Roles of
1130 STAT4 and STAT6 Transcription Factors in Tuning Epigenetic Modifications and Transcription
1131 during T Helper Cell Differentiation. *Immunity* **32,** 840–851 (2010).

1132 81. Onodera, A., Yamashita, M., Endo, Y., Kuwahara, M., Tofukuji, S., Hosokawa, H., Kanai, A.,
1133 Suzuki, Y. & Nakayama, T. STAT6-mediated displacement of polycomb by trithorax complex
1134 establishes long-term maintenance of GATA3 expression in T helper type 2 cells. *J Exp Med*
1135 **207,** 2493–2506 (2010).

1136 82. Barlow, J. L., Peel, S., Fox, J., Panova, V., Hardman, C. S., Camelo, A., Bucks, C., Wu, X.,
1137 Kane, C. M., Neill, D. R., Flynn, R. J., Sayers, I., Hall, I. P. & McKenzie, A. N. J. IL-33 is more
1138 potent than IL-25 in provoking IL-13–producing nuocytes (type 2 innate lymphoid cells) and
1139 airway contraction. *J Allergy Clin Immun* **132,** 933–941 (2013).

1140 83. Molofsky, A. B., Van Gool, F., Liang, H.-E., Van Dyken, S. J., Nussbaum, J. C., Lee, J.,
1141 Bluestone, J. A. & Locksley, R. M. Interleukin-33 and Interferon-γ Counter-Regulate Group 2
1142 Innate Lymphoid Cell Activation during Immune Perturbation. *Immunity* **43,** 161–174 (2015).

1143 84. Oliver, P. M., Cao, X., Worthen, G. S., Shi, P., Briones, N., MacLeod, M., White, J., Kirby,
1144 P., Kappler, J., Marrack, P. & Yang, B. Ndfip1 Protein Promotes the Function of Itch Ubiquitin
1145 Ligase to Prevent T Cell Activation and T Helper 2 Cell-Mediated Inflammation. *Immunity* **25,**
1146 929–940 (2006).

1147 85. Altin, J. A., Daley, S. R., Howitt, J., Rickards, H. J., Batkin, A. K., Horikawa, K., Prasad, S.
1148 J., Nelms, K. A., Kumar, S., Wu, L. C., Tan, S.-S., Cook, M. C. & Goodnow, C. C. Ndfip1
1149 mediates peripheral tolerance to self and exogenous antigen by inducing cell cycle exit in
1150 responding CD4+ T cells. *Proc National Acad Sci* **111,** 2067–2074 (2014).

1151 86. Ferreira, M. A., Matheson, M. C., Duffy, D. L., Marks, G. B., Hui, J., Souëf, P. L., Danoy, P.,
1152 Baltic, S., Nyholt, D. R., Jenkins, M., Hayden, C., Willemsen, G., Ang, W., Kuokkanen, M.,
1153 Beilby, J., Cheah, F., Geus, E. J. de, Ramasamy, A., Vedantam, S., Salomaa, V., Madden, P.
1154 A., Heath, A. C., Hopper, J. L., Visscher, P. M., Musk, B., Leeder, S. R., Jarvelin, M.-R.,
1155 Pennell, C., Boomsma, D. I., Hirschhorn, J. N., Walters, H., Martin, N. G., James, A., Jones, G.,
1156 Abramson, M. J., Robertson, C. F., Dharmage, S. C., Brown, M. A., Montgomery, G. W.,
1157 Thompson, P. J. & Consortium, for the A. A. G. Identification of IL6R and chromosome 11q13.5
1158 as risk loci for asthma. *Lancet* **378,** 1006–1014 (2011).

1159 87. Chi, H., Barry, S. P., Roth, R. J., Wu, J. J., Jones, E. A., Bennett, A. M. & Flavell, R. A.
1160 Dynamic regulation of pro- and anti-inflammatory cytokines by MAPK phosphatase 1 (MKP-1) in
1161 innate immune responses. *Proc National Acad Sci* **103,** 2274–2279 (2006).

1162 88. Clark, A. R., Martins, J. R. S. & Tchen, C. R. Role of Dual Specificity Phosphatases in
1163 Biological Responses to Glucocorticoids*. *J Biol Chem* **283,** 25765–25769 (2008).

1164 89. Grosche, S., Marenholz, I., Esparza-Gordillo, J., Arnau-Soler, A., Pairo-Castineira, E.,
1165 Rüschendorf, F., Ahluwalia, T. S., Almqvist, C., Arnold, A., (AAGC), A. A. G. C., Baurecht, H.,
1166 Bisgaard, H., Bønnelykke, K., Brown, S. J., Bustamante, M., Curtin, J. A., Custovic, A.,
1167 Dharmage, S. C., Esplugues, A., Falchi, M., Fernandez-Orth, D., Ferreira, M. A. R., Franke, A.,
1168 Gerdes, S., Gieger, C., Hakonarson, H., Holt, P. G., Homuth, G., Hubner, N., Hysi, P. G.,

1169 Jarvelin, M.-R., Karlsson, R., Koppelman, G. H., Lau, S., Lutz, M., Magnusson, P. K. E., Marks,
1170 G. B., Müller-Nurasyid, M., Nöthen, M. M., Paternoster, L., Pennell, C. E., Peters, A., Rawlik, K.,
1171 Robertson, C. F., Rodriguez, E., Sebert, S., Simpson, A., Sleiman, P. M. A., Standl, M., Stölzl,
1172 D., Strauch, K., Szwajda, A., Tenesa, A., Thompson, P. J., Ullemar, V., Visconti, A., Vonk, J. M.,
1173 Wang, C. A., Weidinger, S., Wielscher, M., Worth, C. L., Xu, C.-J. & Lee, Y.-A. Rare variant
1174 analysis in eczema identifies exonic variants in DUSP1, NOTCH4 and SLC9A4. *Nat Commun*
1175 **12,** 6618 (2021).

1176 90. Xie, M., Lu, C., Wang, J., McLellan, M. D., Johnson, K. J., Wendl, M. C., McMichael, J. F.,
1177 Schmidt, H. K., Yellapantula, V., Miller, C. A., Ozenberger, B. A., Welch, J. S., Link, D. C.,
1178 Walter, M. J., Mardis, E. R., Dipersio, J. F., Chen, F., Wilson, R. K., Ley, T. J. & Ding, L. Age-
1179 related mutations associated with clonal hematopoietic expansion and malignancies. *Nat Med*
1180 **20,** 1472–1478 (2014).

1181 91. Giulio, G., K., K. A., E., H. R., Johan, L., A., R. S., F., B. S., Kimberly, C., Eran, M., M., N.
1182 B., Menachem, F., M., P. S., Oscar, S., Mikael, L., Martin, H., Sören, L., B., G. S., L., M. J., S.,
1183 L. E., F., S. P., Pamela, S., Henrik, G., M., H. C. & A., M. S. Clonal Hematopoiesis and Blood-
1184 Cancer Risk Inferred from Blood DNA Sequence. *New Engl J Med* **371,** 2477–2487 (2014).

1185 92. Siddhartha, J., Pierre, F., Jason, F., Alisa, M., V., G. P., G., M. B., Coleman, L. R., H., M. C.,
1186 Noel, B., Alejandro, C., M., H. J., Vladislav, M., C., K. F., J., K. M., Brian, H., Leena, K., A., K.
1187 H., Claes, L., Gad, G., Adolfo, C., F., B. B., Stacey, G., Sekar, K., M., S. H., I., M. M., Michael,
1188 B., Jaakko, T., Christopher, H., Leif, G., Gil, A., G., W. J., Donna, N., David, A. & L., E. B. Age-
1189 Related Clonal Hematopoiesis Associated with Adverse Outcomes. *New Engl J Med* **371,**
1190 2488–2498 (2014).

1191 93. Nagase, R., Inoue, D., Pastore, A., Fujino, T., Hou, H.-A., Yamasaki, N., Goyama, S., Saika,
1192 M., Kanai, A., Sera, Y., Horikawa, S., Ota, Y., Asada, S., Hayashi, Y., Kawabata, K. C., Takeda,
1193 R., Tien, H.-F., Honda, H., Abdel-Wahab, O. & Kitamura, T. Expression of mutant Asxl1
1194 perturbs hematopoiesis and promotes susceptibility to leukemic transformation. *J Exp Med* **215,**
1195 1729–1747 (2018).

1196 94. Kobayashi, T., Voisin, B., Kim, D. Y., Kennedy, E. A., Jo, J.-H., Shih, H.-Y., Truong, A.,
1197 Doebel, T., Sakamoto, K., Cui, C.-Y., Schlessinger, D., Moro, K., Nakae, S., Horiuchi, K., Zhu,
1198 J., Leonard, W. J., Kong, H. H. & Nagao, K. Homeostatic Control of Sebaceous Glands by
1199 Innate Lymphoid Cells Regulates Commensal Bacteria Equilibrium. *Cell* **176,** 982-997.e16
1200 (2019).

1201 95. Lee, G. R., Fields, P. E., Griffin, T. J. & Flavell, R. A. Regulation of the Th2 Cytokine Locus
1202 by a Locus Control Region. *Immunity* **19,** 145–153 (2003).

1203 96. Loots, G. G., Locksley, R. M., Blankespoor, C. M., Wang, Z. E., Miller, W., Rubin, E. M. &
1204 Frazer, K. A. Identification of a Coordinate Regulator of Interleukins 4, 13, and 5 by Cross-
1205 Species Sequence Comparisons. *Science* **288,** 136–140 (2000).

1206 97. Fields, P. E., Lee, G. R., Kim, S. T., Bartsevich, V. V. & Flavell, R. A. Th2-Specific
1207 Chromatin Remodeling and Enhancer Activity in the Th2 Cytokine Locus Control Region.
1208 *Immunity* **21,** 865–876 (2004).

1209 98. Zhang, Y., Cheng, T. C., Huang, G., Lu, Q., Surleac, M. D., Mandell, J. D., Pontarotti, P.,
1210 Petrescu, A. J., Xu, A., Xiong, Y. & Schatz, D. G. Transposon molecular domestication and the
1211 evolution of the RAG recombinase. *Nature* **569,** 79–84 (2019).

1212 99. Buckley, R. H. Molecular Defects in Human Severe Combined Immunodeficiency and
1213 Approaches to Immune Reconstitution. *Annu Rev Immunol* **22,** 625–655 (2004).

1214 100. Mombaerts, P., Iacomini, J., Johnson, R. S., Herrup, K., Tonegawa, S. & Papaioannou, V.
1215 E. RAG-1-deficient mice have no mature B and T lymphocytes. *Cell* **68,** 869–877 (1992).

1216 101. Shinkai, Y., Rathbun, 0Gary, Lam, K.-P., Oltz, E. M., Stewart, V., Mendelsohn, M.,
1217 Charron, J., Datta, M., Young, F., Stall, A. M. & Alt, F. W. RAG-2-deficient mice lack mature
1218 lymphocytes owing to inability to initiate V(D)J rearrangement. *Cell* **68,** 855–867 (1992).

1219 102. Igarashi, H., Gregory, S. C., Yokota, T., Sakaguchi, N. & Kincade, P. W. Transcription from
1220 the RAG1 Locus Marks the Earliest Lymphocyte Progenitors in Bone Marrow. *Immunity* **17,**
1221 117–130 (2002).

1222 103. Pelayo, R., Hirose, J., Huang, J., Garrett, K. P., Delogu, A., Busslinger, M. & Kincade, P.
1223 W. Derivation of 2 categories of plasmacytoid dendritic cells in murine bone marrow. *Blood* **105,**
1224 4407–4415 (2005).

1225 104. Wilson, A., Held, W. & MacDonald, H. R. Two waves of recombinase gene expression in
1226 developing thymocytes. *J Exp Medicine* **179,** 1355–1360 (1994).

1227 105. Zhu, J., Yamane, H. & Paul, W. E. Differentiation of Effector CD4 T Cell Populations*.
1228 *Annu Rev Immunol* **28,** 445–489 (2010).

1229 106. Koues, O. I., Collins, P. L., Cella, M., Robinette, M. L., Porter, S. I., Pyfrom, S. C., Payton,
1230 J. E., Colonna, M. & Oltz, E. M. Distinct Gene Regulatory Pathways for Human Innate versus
1231 Adaptive Lymphoid Cells. *Cell* **165,** 1134–1146 (2016).

1232 107. Agarwal, S. & Rao, A. Modulation of Chromatin Structure Regulates Cytokine Gene
1233 Expression during T Cell Differentiation. *Immunity* **9,** 765–775 (1998).

1234 108. Omenn, G. S. Familial Reticuloendotheliosis with Eosinophilia. *New Engl J Medicine* **273,**
1235 427–432 (1965).

1236 109. Villa, A., Notarangelo, L. D. & Roifman, C. M. Omenn syndrome: inflammation in leaky
1237 severe combined immunodeficiency. *J Allergy Clin Immun* **122,** 1082–1086 (2008).

1238 110. Villa, A., Santagata, S., Bozzi, F., Giliani, S., Frattini, A., Imberti, L., Gatta, L. B., Ochs, H.
1239 D., Schwarz, K., Notarangelo, L. D., Vezzoni, P. & Spanopoulou, E. Partial V(D)J recombination
1240 activity leads to Omenn syndrome. *Cell* **93,** 885–896 (1998).

1241 111. Villa, A., Sobacchi, C., Notarangelo, L. D., Bozzi, F., Abinun, M., Abrahamsen, T. G.,
1242 Arkwright, P. D., Baniyash, M., Brooks, E. G., Conley, M. E., Cortes, P., Duse, M., Fasth, A.,
1243 Filipovich, A. M., Infante, A. J., Jones, A., Mazzolari, E., Muller, S. M., Pasic, S., Rechavi, G.,
1244 Sacco, M. G., Santagata, S., Schroeder, M. L., Seger, R., Strina, D., Ugazio, A., Väliaho, J.,

1245 Vihinen, M., Vogler, L. B., Ochs, H., Vezzoni, P., Friedrich, W. & Schwarz, K. V(D)J
1246 recombination defects in lymphocytes due to RAG mutations: severe immunodeficiency with a
1247 spectrum of clinical presentations. *Blood* **97,** 81–88 (2001).

1248 112. Wada, T., Toma, T., Okamoto, H., Kasahara, Y., Koizumi, S., Agematsu, K., Kimura, H.,
1249 Shimada, A., Hayashi, Y., Kato, M. & Yachie, A. Oligoclonal expansion of T lymphocytes with
1250 multiple second-site mutations leads to Omenn syndrome in a patient with RAG1-deficient
1251 severe combined immunodeficiency. *Blood* **106,** 2099–2101 (2005).

1252 113. Marrella, V., Poliani, P. L., Casati, A., Rucci, F., Frascoli, L., Gougeon, M.-L., Lemercier,
1253 B., Bosticardo, M., Ravanini, M., Battaglia, M., Roncarolo, M. G., Cavazzana-Calvo, M.,
1254 Facchetti, F., Notarangelo, L. D., Vezzoni, P., Grassi, F. & Villa, A. A hypomorphic R229Q Rag2
1255 mouse mutant recapitulates human Omenn syndrome. *J Clin Invest* **117,** 1260–1269 (2007).

1256 114. Khiong, K., Murakami, M., Kitabayashi, C., Ueda, N., Sawa, S., Sakamoto, A., Kotzin, B.
1257 L., Rozzo, S. J., Ishihara, K., Verella-Garcia, M., Kappler, J., Marrack, P. & Hirano, T.
1258 Homeostatically proliferating CD4+ T cells are involved in the pathogenesis of an Omenn
1259 syndrome murine model. *J Clin Invest* **117,** 1270–1281 (2007).

1260 115. Milner, J. D., Ward, J. M., Keane-Myers, A. & Paul, W. E. Lymphopenic mice reconstituted
1261 with limited repertoire T cells develop severe, multiorgan, Th2-associated inflammatory disease.
1262 *Proc. Natl. Acad. Sci.* **104,** 576–581 (2007).

1263 116. Pike-Overzet, K., Rodijk, M., Ng, Y.-Y., Baert, M. R. M., Lagresle-Peyrou, C., Schambach,
1264 A., Zhang, F., Hoeben, R. C., Hacein-Bey-Abina, S., Lankester, A. C., Bredius, R. G. M.,
1265 Driessen, G. J. A., Thrasher, A. J., Baum, C., Cavazzana-Calvo, M., Dongen, J. J. M. van &
1266 Staal, F. J. T. Correction of murine Rag1 deficiency by self-inactivating lentiviral vector-
1267 mediated gene transfer. *Leukemia* **25,** 1471–1483 (2011).

1268 117. Pike-Overzet, K., Baum, C., Bredius, R. G. M., Cavazzana, M., Driessen, G.-J., Fibbe, W.
1269 E., Gaspar, H. B., Hoeben, R. C., Lagresle-Peyrou, C., Lankester, A., Meij, P., Schambach, A.,
1270 Thrasher, A., Dongen, J. J. M. V., Zwaginga, J.-J. & Staal, F. J. T. Successful RAG1-SCID gene
1271 therapy depends on the level of RAG1 expression. *J Allergy Clin Immun* **134,** 242–243 (2014).

1272 118. Til, N. P. van, Cortes, P., Danos, O., Cassani, B., Poliani, P. L., Villa, A. & Wagemaker, G.
1273 Reply. *J Allergy Clin Immun* **134,** 243–244 (2014).

1274 119. Til, N. P. van, Sarwari, R., Visser, T. P., Hauer, J., Lagresle-Peyrou, C., Velden, G. van
1275 der, Malshetty, V., Cortes, P., Jollet, A., Danos, O., Cassani, B., Zhang, F., Thrasher, A. J.,
1276 Fontana, E., Poliani, P. L., Cavazzana, M., Verstegen, M. M. A., Villa, A. & Wagemaker, G.
1277 Recombination-activating gene 1 (Rag1)–deficient mice with severe combined
1278 immunodeficiency treated with lentiviral gene therapy demonstrate autoimmune Omenn-like
1279 syndrome. *J Allergy Clin Immun* **133,** 1116–1123 (2014).

1280 120. Schatz, D. G. & Swanson, P. C. V(D)J Recombination: Mechanisms of Initiation. *Annu Rev*
1281 *Genet* **45,** 167–202 (2011).

1282 121. Kuo, T. C. & Schlissel, M. S. Mechanisms controlling expression of the RAG locus during
1283 lymphocyte development. *Curr Opin Immunol* **21,** 173–178 (2009).

1284 122. Desiderio, S. Temporal and spatial regulatory functions of the V(D)J recombinase. *Semin*
1285 *Immunol* **22,** 362–369 (2010).

1286 123. Young, M. D. & Behjati, S. SoupX removes ambient RNA contamination from droplet-
1287 based single-cell RNA sequencing data. *Gigascience* **9,** giaa151 (2020).

1288 124. Wolock, S. L., Lopez, R. & Klein, A. M. Scrublet: Computational Identification of Cell
1289 Doublets in Single-Cell Transcriptomic Data. *Cell Syst* **8,** 281-291.e9 (2019).

1290 125. Zhang, Y., Liu, T., Meyer, C. A., Eeckhoute, J., Johnson, D. S., Bernstein, B. E., Nusbaum,
1291 C., Myers, R. M., Brown, M., Li, W. & Liu, X. S. Model-based Analysis of ChIP-Seq (MACS).
1292 *Genome Biol* **9,** R137 (2008).

1293 126. Ntranos, V., Yi, L., Melsted, P. & Pachter, L. A discriminative learning approach to
1294 differential expression analysis for single-cell RNA-seq. *Nat Methods* **16,** 163–166 (2019).

1295 127. Hulsen, T., Vlieg, J. de & Alkema, W. BioVenn – a web application for the comparison and
1296 visualization of biological lists using area-proportional Venn diagrams. *Bmc Genomics* **9,** 488
1297 (2008).

1298 128. Wu, T., Hu, E., Xu, S., Chen, M., Guo, P., Dai, Z., Feng, T., Zhou, L., Tang, W., Zhan, L.,
1299 Fu, X., Liu, S., Bo, X. & Yu, G. clusterProfiler 4.0: A universal enrichment tool for interpreting
1300 omics data. *Innovation* **2,** 100141 (2021).

1301 129. Conway, J. R., Lex, A. & Gehlenborg, N. UpSetR: an R package for the visualization of
1302 intersecting sets and their properties. *Bioinformatics* **33,** 2938–2940 (2017).

1303 130. Schep, A. N., Wu, B., Buenrostro, J. D. & Greenleaf, W. J. chromVAR: inferring
1304 transcription-factor-associated accessibility from single-cell epigenomic data. *Nat Methods* **14,**
1305 975–978 (2017).

1306 131. Wang, Y., Sarfraz, I., Hong, R., Koga, Y., Alabdullatif, S., Jenkins, D., Akavoor, V., Cao, X.,
1307 Bandyadka, S., Leshchyk, A., Faits, T., Khan, M. M., Wang, Z., Johnson, W. E. & Campbell, J.
1308 D. singleCellTK: Comprehensive and Interactive Analysis of Single Cell RNA-Seq Data.
1309 (2022). at <https://www.camplab.net/sctk/>;

1310 132. Durinck, S., Spellman, P. T., Birney, E. & Huber, W. Mapping identifiers for the integration
1311 of genomic datasets with the R/Bioconductor package biomaRt. *Nat Protoc* **4,** 1184–1191
1312 (2009).

1313 133. Rainer, J. EnsDb.Mmusculus.v79: Ensembl based annotation package. (2017).

1314 134. TBD, T. BSgenome.Mmusculus.UCSC.mm10: Full genome sequences for Mus musculus
1315 (UCSC version mm10, based on GRCm38.p6). (2021).

1316 135. Wickham, H. ggplot2: Elegant Graphics for Data Analysis. (2016). at
1317 <https://ggplot2.tidyverse.org>;

136. Garnier, Simon, Ross, Noam, Rudis, Robert, Camargo, Pedro, A., Sciaini, Marco, Scherer & Cédric. viridis - Colorblind-Friendly Color Maps for R. (2021). doi:10.5281/zenodo.4679424

137. Tan, G. & Lenhard, B. TFBSTools: an R/bioconductor package for transcription factor binding site analysis. *Bioinformatics* **32,** 1555–1556 (2016).

138. Schep, A. motifmatchr: Fast Motif Matching in R. (2022).

139. Zheng, G. X. Y., Terry, J. M., Belgrader, P., Ryvkin, P., Bent, Z. W., Wilson, R., Ziraldo, S. B., Wheeler, T. D., McDermott, G. P., Zhu, J., Gregory, M. T., Shuga, J., Montesclaros, L., Underwood, J. G., Masquelier, D. A., Nishimura, S. Y., Schnall-Levin, M., Wyatt, P. W., Hindson, C. M., Bharadwaj, R., Wong, A., Ness, K. D., Beppu, L. W., Deeg, H. J., McFarland, C., Loeb, K. R., Valente, W. J., Ericson, N. G., Stevens, E. A., Radich, J. P., Mikkelsen, T. S., Hindson, B. J. & Bielas, J. H. Massively parallel digital transcriptional profiling of single cells. *Nat Commun* **8,** 14049 (2017).

140. Satpathy, A. T., Granja, J. M., Yost, K. E., Qi, Y., Meschi, F., McDermott, G. P., Olsen, B. N., Mumbach, M. R., Pierce, S. E., Corces, M. R., Shah, P., Bell, J. C., Jhutty, D., Nemec, C. M., Wang, J., Wang, L., Yin, Y., Giresi, P. G., Chang, A. L. S., Zheng, G. X. Y., Greenleaf, W. J. & Chang, H. Y. Massively parallel single-cell chromatin landscapes of human immune cell development and intratumoral T cell exhaustion. *Nat Biotechnol* **37,** 925–936 (2019).

Figure 1

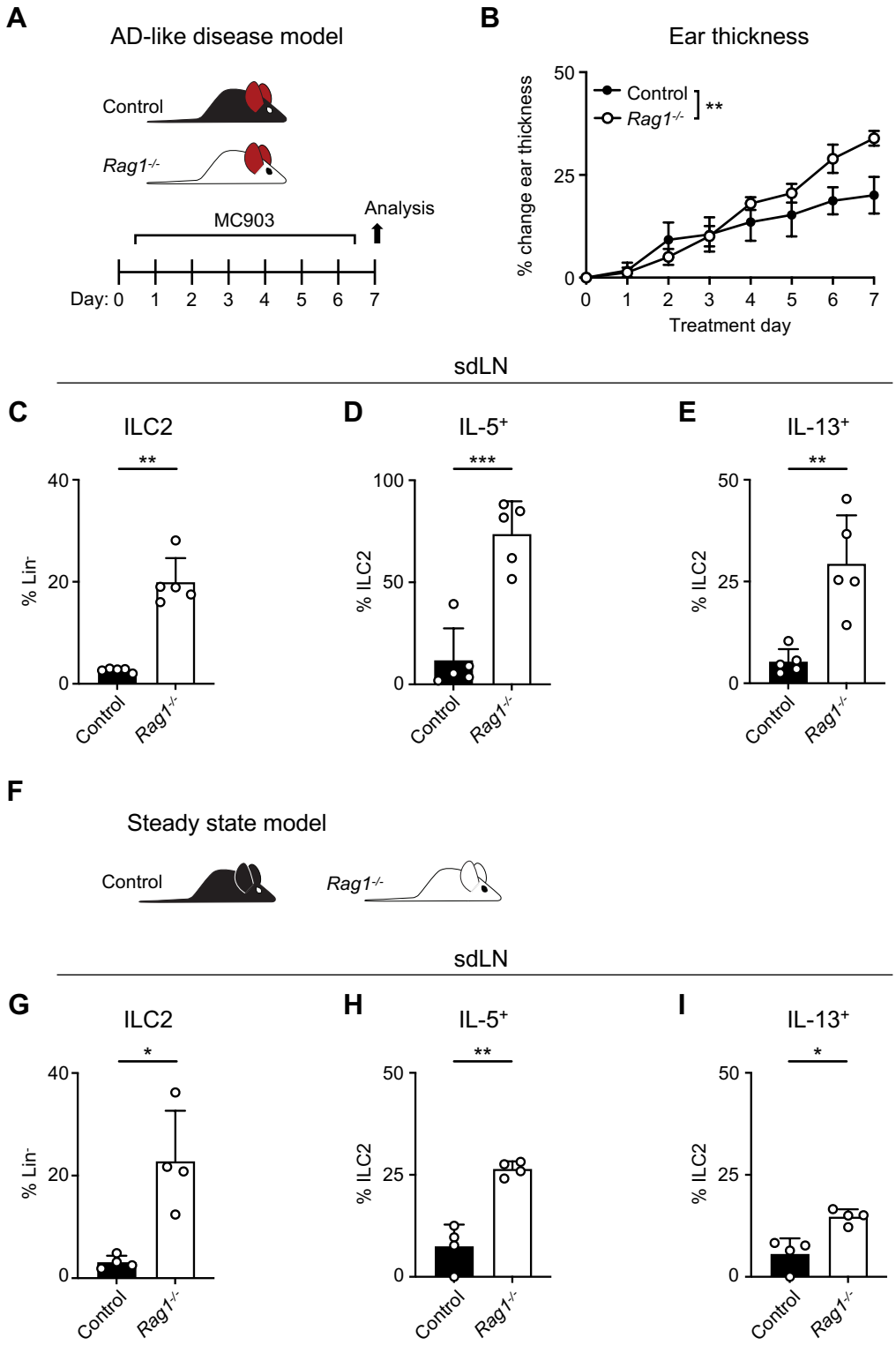
A
AD-like disease model
Control
Rag1-/-
MC903
Analysis
Day: 0 1 2 3 4 5 6 7
B
Ear thickness
Control
Rag1-/-
**
% change ear thickness
Treatment day
sdLN
C
ILC2
**
% Lin-
Control
Rag1-/-
D
IL-5+
***
% ILC2
E
IL-13+
**
F
Steady state model
Control
Rag1-/-
sdLN
G
ILC2
*
H
IL-5+
**
I
IL-13+
*

Figure 2

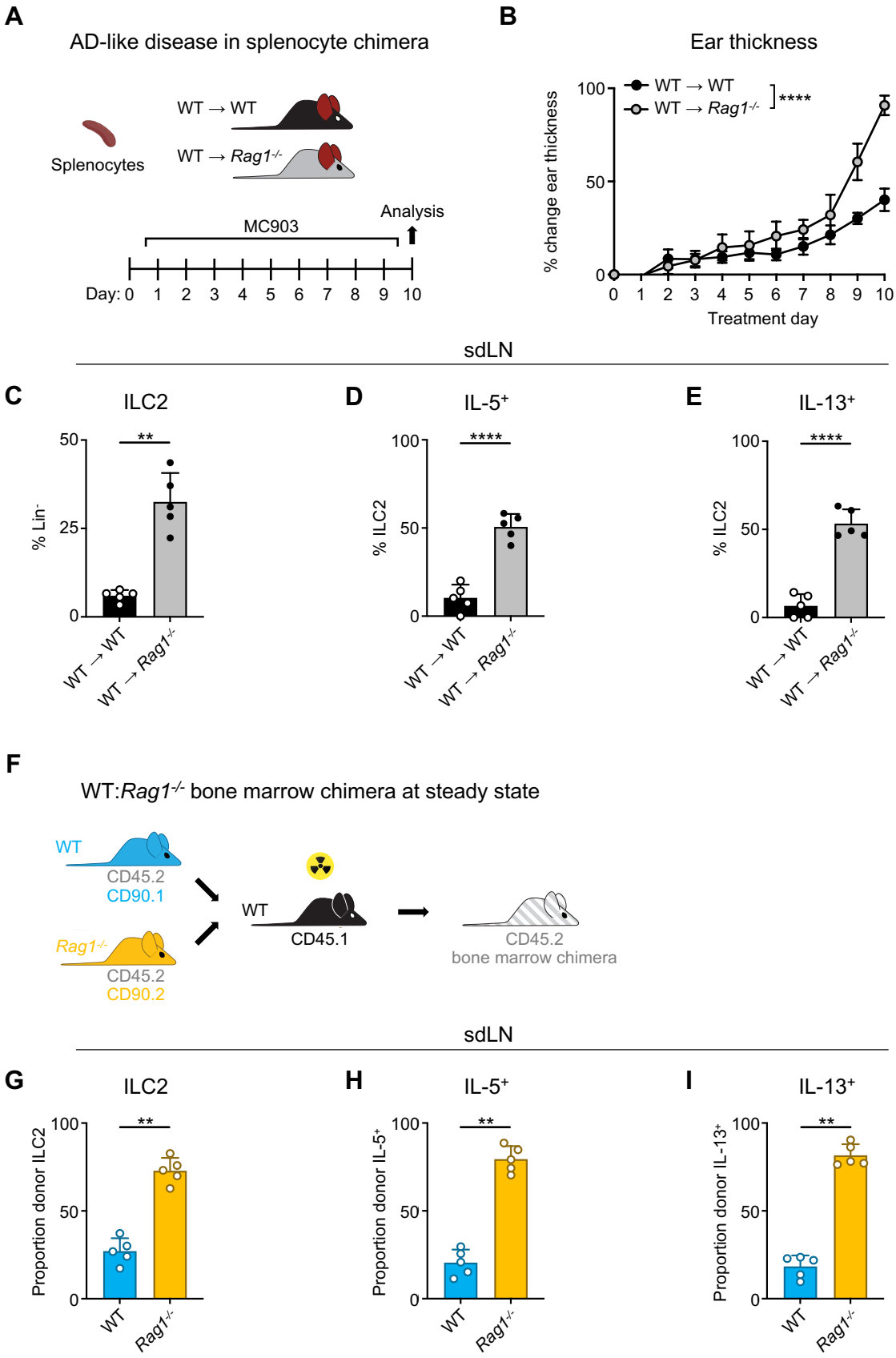
A
AD-like disease in splenocyte chimera
Splenocytes
WT → WT
WT → Rag1-/-
MC903
Analysis
Day: 0 1 2 3 4 5 6 7 8 9 10
B
Ear thickness
WT → WT
WT → Rag1-/-
****
% change ear thickness
Treatment day
sdLN
C
ILC2
% Lin-
**
D
IL-5+
% ILC2
****
E
IL-13+
% ILC2
****
F
WT:Rag1-/- bone marrow chimera at steady state
WT
CD45.2
CD90.1
Rag1-/-
CD45.2
CD90.2
WT
CD45.1
CD45.2
bone marrow chimera
sdLN
G
ILC2
Proportion donor ILC2
**
H
IL-5+
Proportion donor IL-5+
**
I
IL-13+
Proportion donor IL-13+
**
WT
Rag1-/-

Figure 3

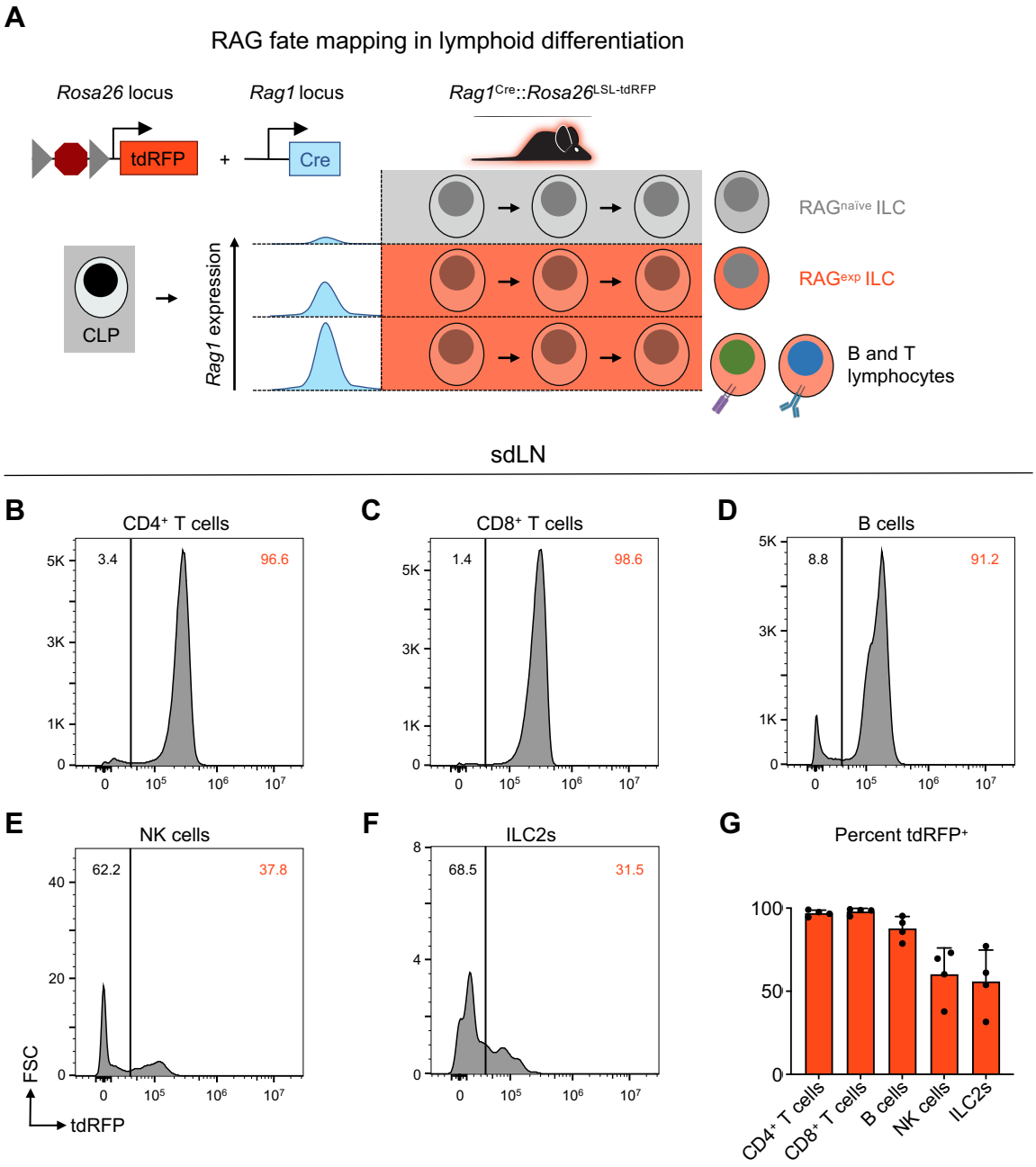
A
RAG fate mapping in lymphoid differentiation
Rosa26 locus
Rag1 locus
Rag1Cre::Rosa26LSL-tdRFP
tdRFP
Cre
CLP
Rag1 expression
RAGnaïve ILC
RAGexp ILC
B and T lymphocytes
sdLN
B
CD4+ T cells
3.4
96.6
C
CD8+ T cells
1.4
98.6
D
B cells
8.8
91.2
E
NK cells
62.2
37.8
FSC
tdRFP
F
ILC2s
68.5
31.5
G
Percent tdRFP+
CD4+ T cells
CD8+ T cells
B cells
NK cells
ILC2s

Figure 4

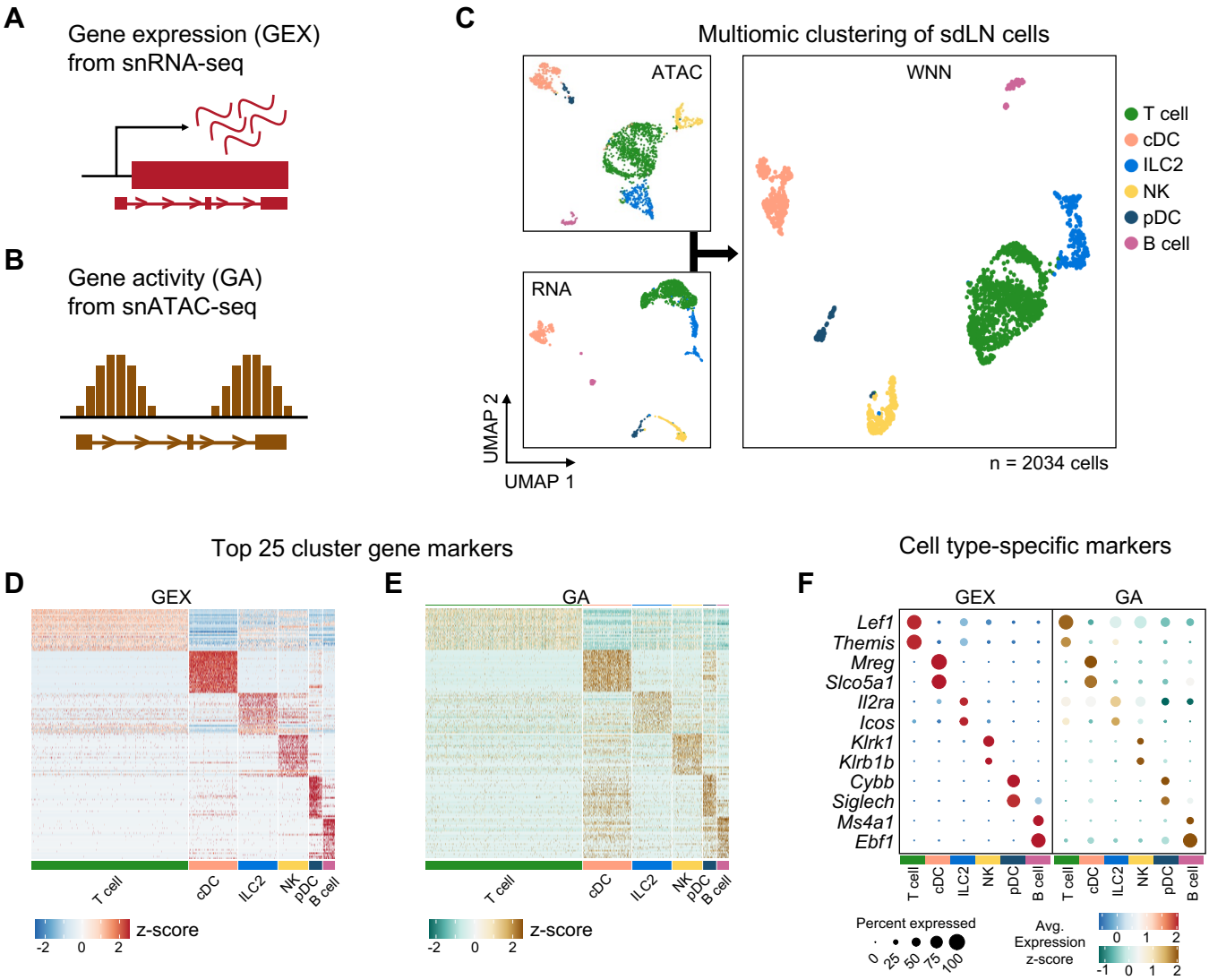
A
Gene expression (GEX)
from snRNA-seq
B
Gene activity (GA)
from snATAC-seq
C
Multiomic clustering of sdLN cells
ATAC
RNA
WNN
T cell
cDC
ILC2
NK
pDC
B cell
UMAP 2
UMAP 1
n = 2034 cells
Top 25 cluster gene markers
D
GEX
E
GA
T cell
cDC
ILC2
NK
pDC
B cell
z-score
-2
0
2
Cell type-specific markers
F
GEX
GA
Lef1
Themis
Mreg
Slco5a1
Il2ra
Icos
Klrk1
Klrb1b
Cybb
Siglech
Ms4a1
Ebf1
Percent expressed
0
25
50
75
100
Avg.
Expression
z-score
-1
0
1
2
G
Differentially accessible (DA)
chromatin to nearest gene
from snATAC-seq
C1
C2
C3
H
ILC2 marker
gene set overlap
Top 100
GEX
Top 100
GA
Top 100
DA
64
15
5
16
56
13
66
n = 235
unique
genes
I
Multiomic ILC2 gene set
Single assay
Dual overlap
Full overlap
Il2ra
Runx1
S100a6
Il18r1
Itgb7
GEX
Bmp7
Il9r
Il1rl1
Ccl1
GA
Il10
Nmur1
Areg
Il5
Il4
DA
Maf
Icos
Gata3
Bcl11b
Ets1
GEX
+
GA
Rora
Itgav
GEX
+
DA
Ccr8
Cish
GA
+
DA
Ptpn13
Tox
GEX
+
GA
+
DA

Figure 5

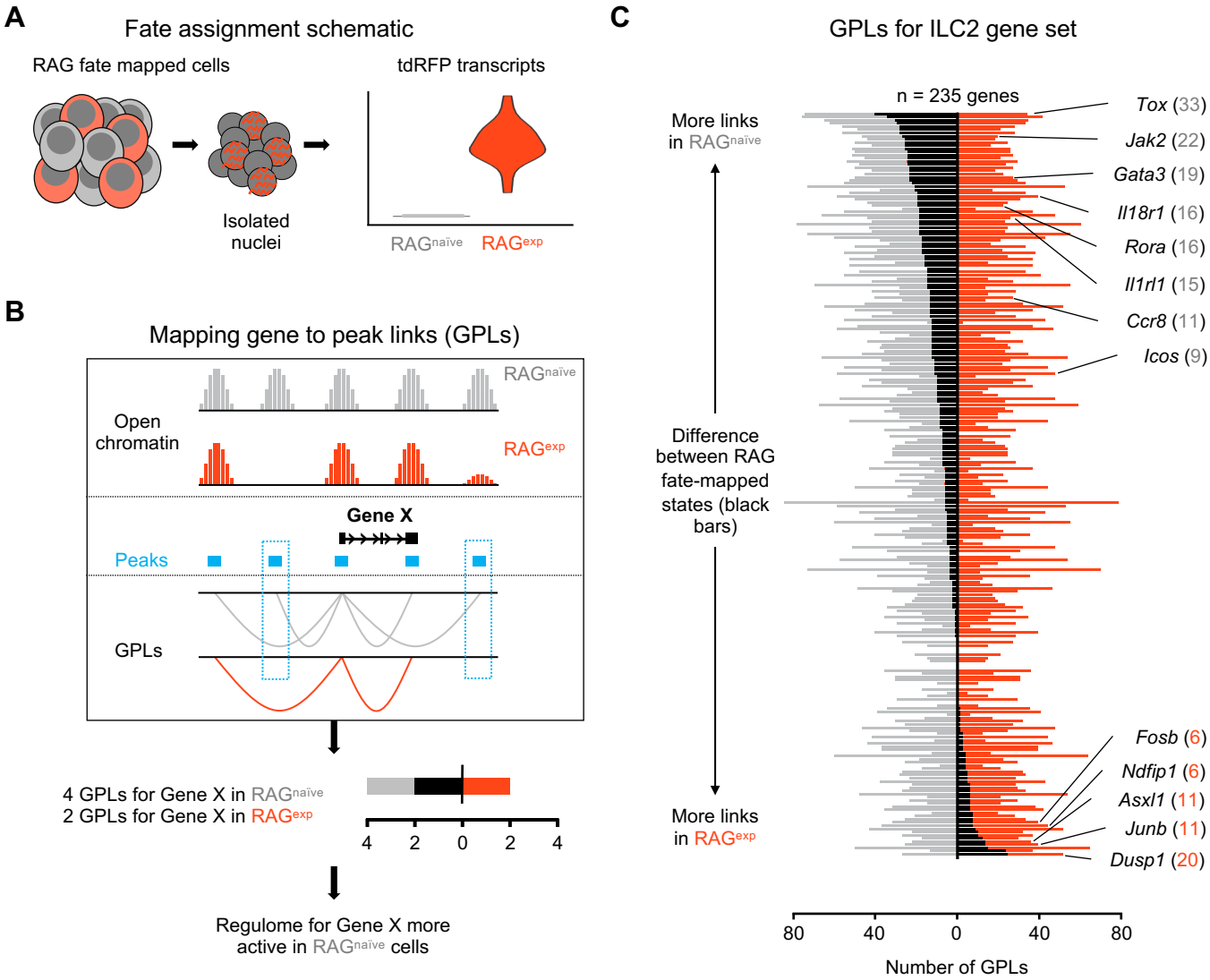
A
Fate assignment schematic
RAG fate mapped cells
tdRFP transcripts
Isolated nuclei
RAGnaïve
RAGexp
B
Mapping gene to peak links (GPLs)
Open chromatin
RAGnaïve
RAGexp
Gene X
Peaks
GPLs
4 GPLs for Gene X in RAGnaïve
2 GPLs for Gene X in RAGexp
4 2 0 2 4
Regulome for Gene X more active in RAGnaïve cells
C
GPLs for ILC2 gene set
n = 235 genes
More links in RAGnaïve
Difference between RAG fate-mapped states (black bars)
More links in RAGexp
Tox (33)
Jak2 (22)
Gata3 (19)
Il18r1 (16)
Rora (16)
Il1rl1 (15)
Ccr8 (11)
Icos (9)
Fosb (6)
Ndfip1 (6)
Asxl1 (11)
Junb (11)
Dusp1 (20)
80 40 0 40 80
Number of GPLs

Figure 6

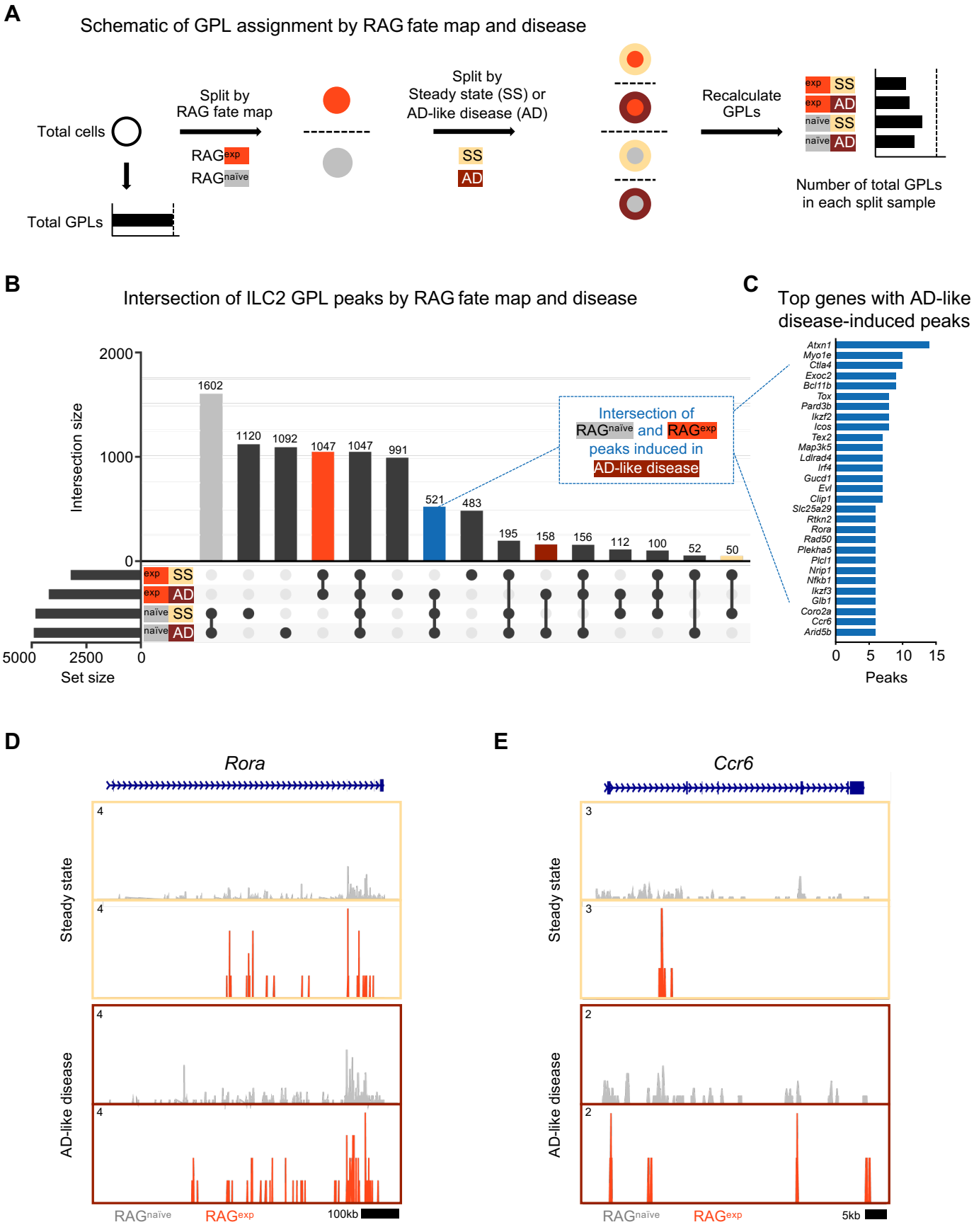
A
Schematic of GPL assignment by RAG fate map and disease
Total cells
Total GPLs
Split by
RAG fate map
RAGexp
RAGnaïve
Split by
Steady state (SS) or
AD-like disease (AD)
SS
AD
Recalculate
GPLs
exp SS
exp AD
naïve SS
naïve AD
Number of total GPLs
in each split sample
B
Intersection of ILC2 GPL peaks by RAG fate map and disease
Intersection size
2000
1000
0
1602
1120
1092
1047
1047
991
521
483
195
158
156
112
100
52
50
Intersection of
RAGnaïve and RAGexp
peaks induced in
AD-like disease
5000
2500
0
Set size
C
Top genes with AD-like
disease-induced peaks
Atxn1
Myo1e
Ctla4
Exoc2
Bcl11b
Tox
Pard3b
Ikzf2
Icos
Tex2
Map3k5
Ldlrad4
Irf4
Gucd1
Evl
Clip1
Slc25a29
Rtkn2
Rora
Rad50
Plekha5
Plcl1
Nrip1
Nfkb1
Ikzf3
Glb1
Coro2a
Ccr6
Arid5b
0
5
10
15
Peaks
D
Rora
Steady state
AD-like disease
RAGnaïve
RAGexp
100kb
E
Ccr6
Steady state
AD-like disease
RAGnaïve
RAGexp
5kb

Figure 7

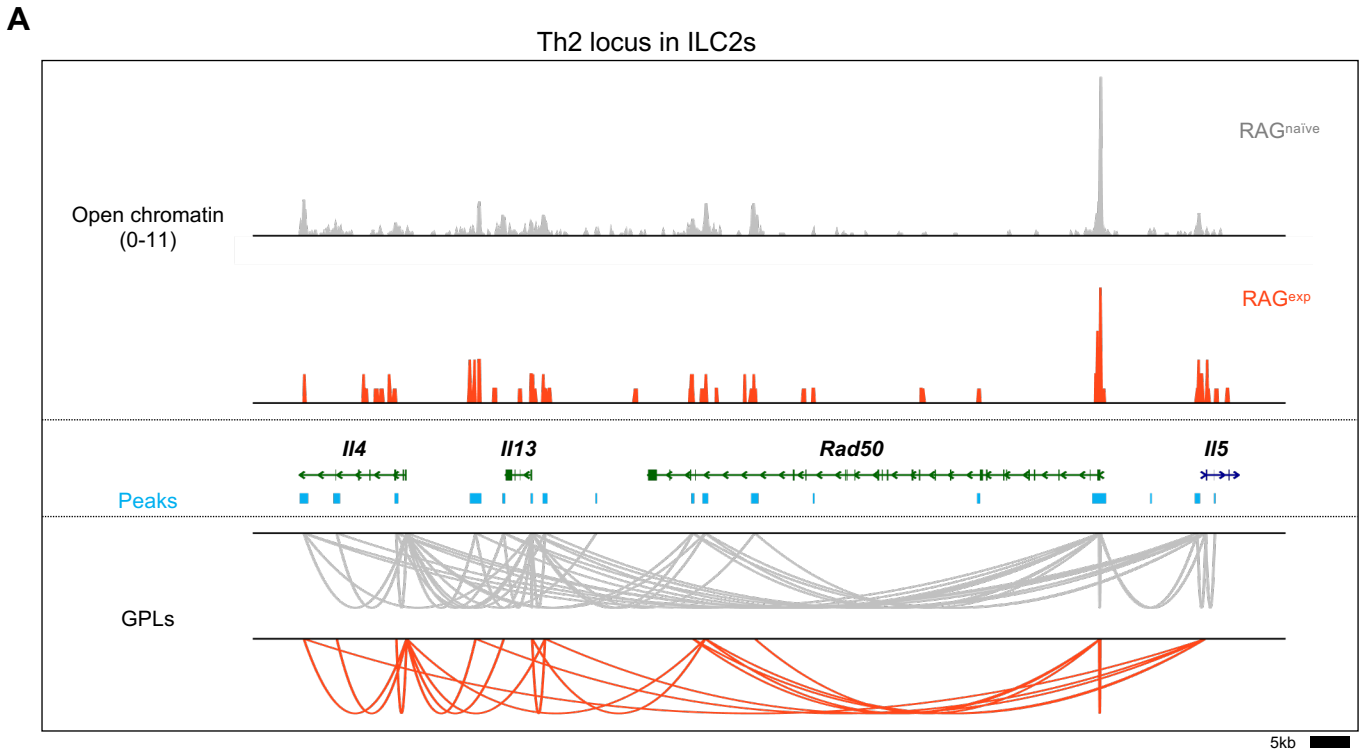
A
Th2 locus in ILC2s
RAGnaïve
Open chromatin
(0-11)
RAGexp
Il4
Il13
Rad50
Il5
Peaks
GPLs
5kb

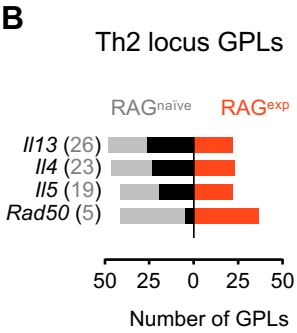
B
Th2 locus GPLs
RAGnaïve
RAGexp
Il13 (26)
Il4 (23)
Il5 (19)
Rad50 (5)
50 25 0 25 50
Number of GPLs

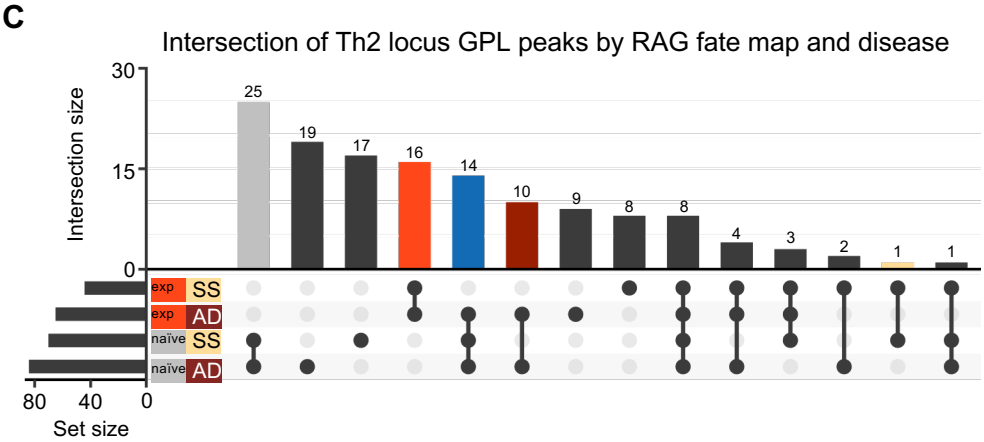
C
Intersection of Th2 locus GPL peaks by RAG fate map and disease
Intersection size
30
15
0
25
19
17
16
14
10
9
8
8
4
3
2
1
1
exp SS
exp AD
naïve SS
naïve AD
80 40 0
Set size

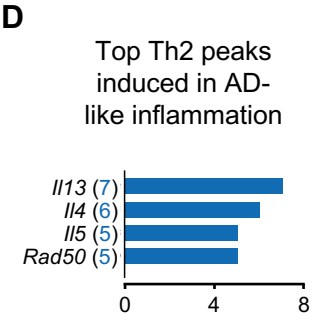
D
Top Th2 peaks
induced in AD-
like inflammation
Il13 (7)
Il4 (6)
Il5 (5)
Rad50 (5)
0 4 8

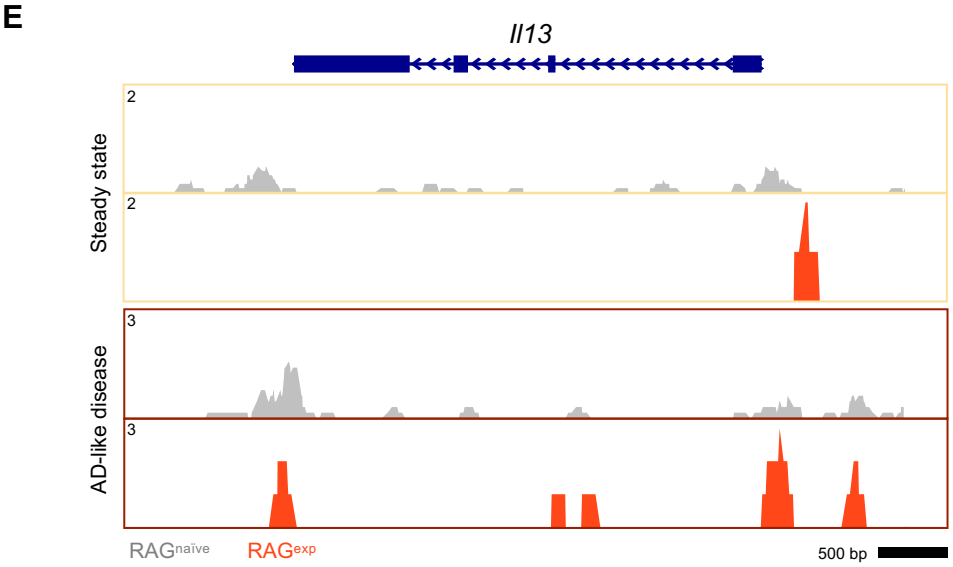
E
Il13
Steady state
2
2
AD-like disease
3
3
RAGnaïve
RAGexp
500 bp

Figure S1

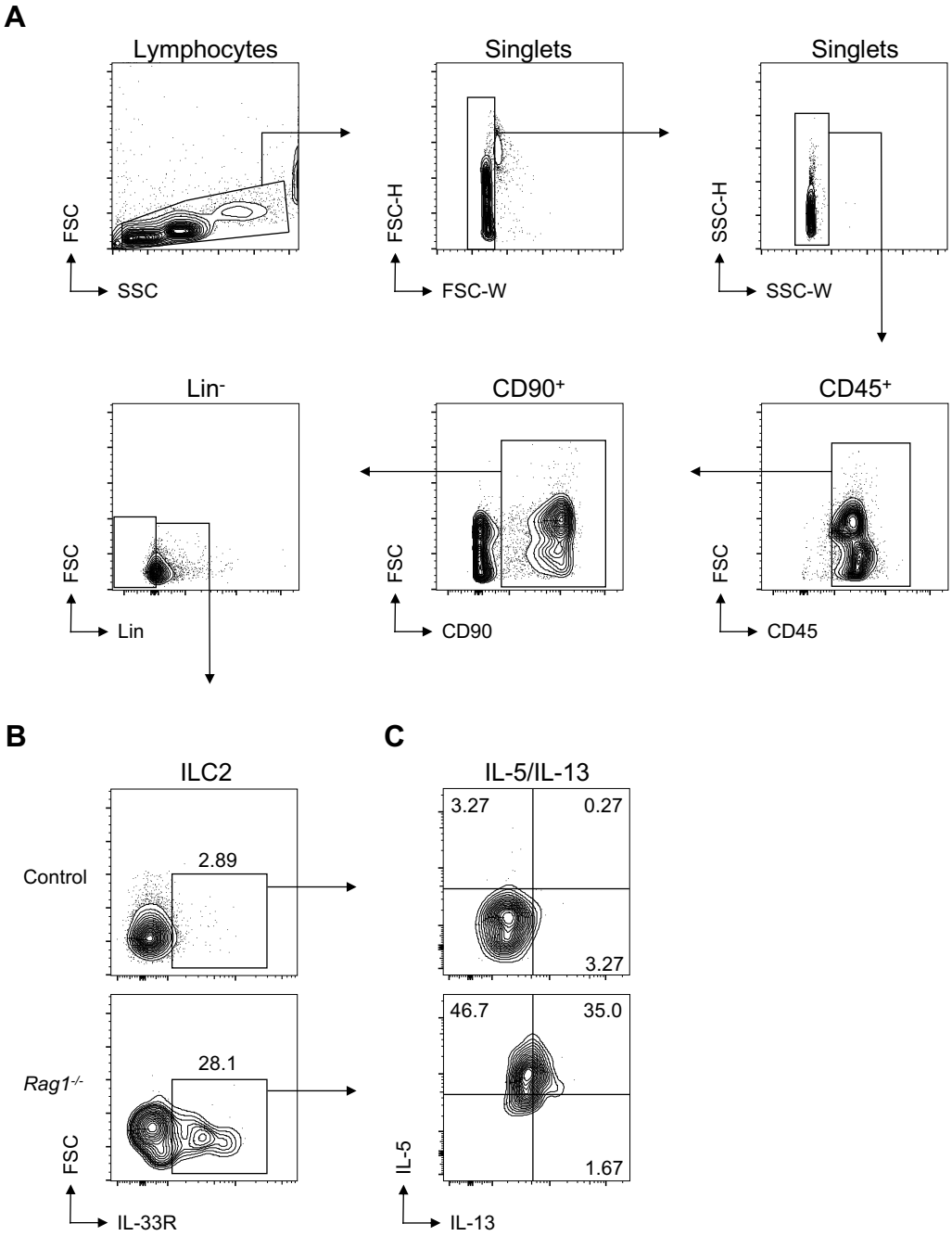
A
Lymphocytes
FSC
SSC
Singlets
FSC-H
FSC-W
Singlets
SSC-H
SSC-W
Lin-
FSC
Lin
CD90+
FSC
CD90
CD45+
FSC
CD45
B
ILC2
Control
2.89
Rag1-/-
28.1
FSC
IL-33R
C
IL-5/IL-13
3.27
0.27
3.27
46.7
35.0
1.67
IL-5
IL-13

Figure S2

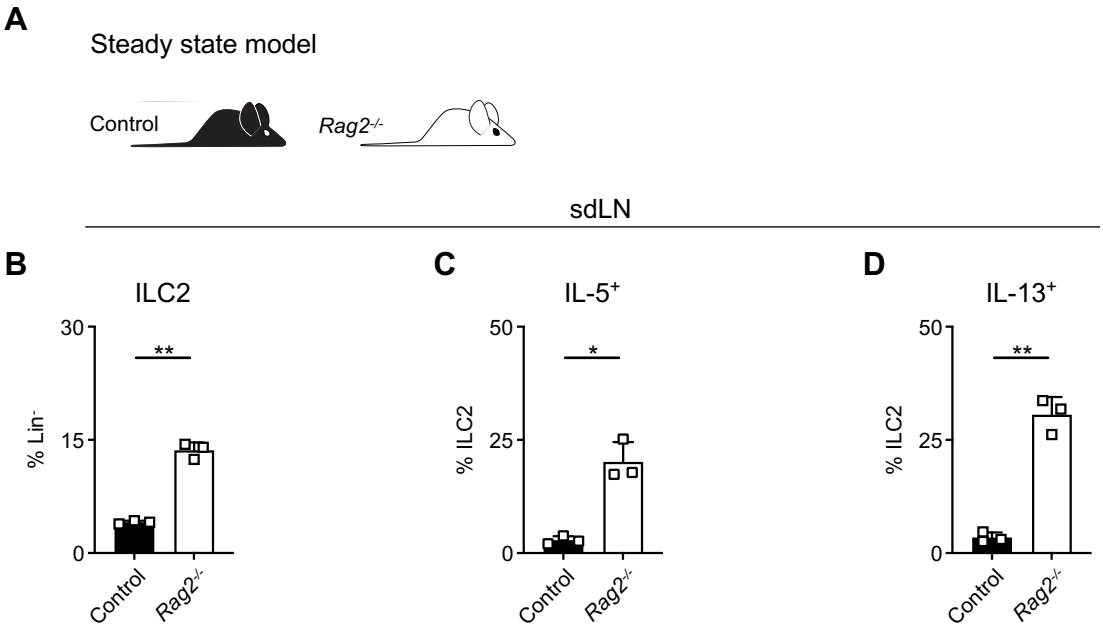
A
Steady state model
Control
Rag2-/-
sdLN
B
ILC2
% Lin-
30
15
0
**
Control
Rag2-/-
C
IL-5+
% ILC2
50
25
0
*
Control
Rag2-/-
D
IL-13+
% ILC2
50
25
0
**
Control
Rag2-/-

Figure S3

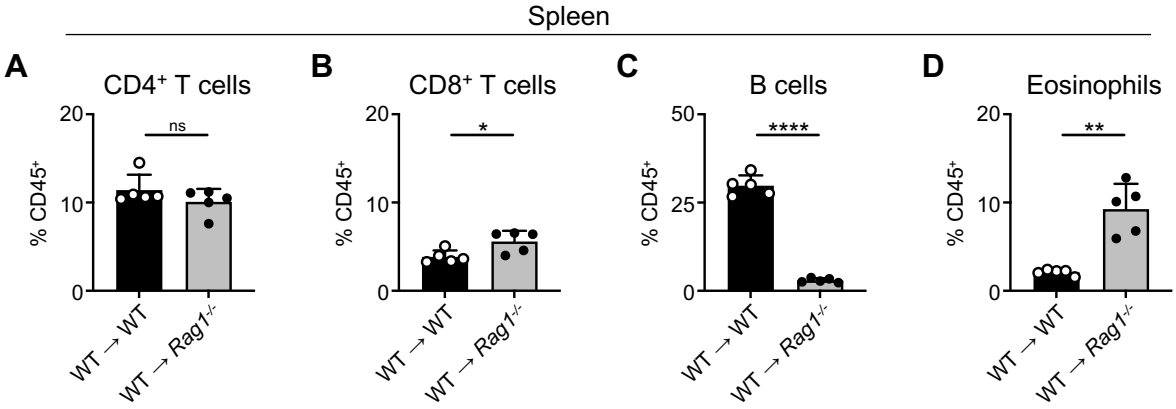
Spleen
A
CD4+ T cells
% CD45+
20
10
0
ns
WT → WT
WT → Rag1-/-
B
CD8+ T cells
% CD45+
20
10
0
*
WT → WT
WT → Rag1-/-
C
B cells
% CD45+
50
25
0
****
WT → WT
WT → Rag1-/-
D
Eosinophils
% CD45+
20
10
0
**
WT → WT
WT → Rag1-/-

Figure S4

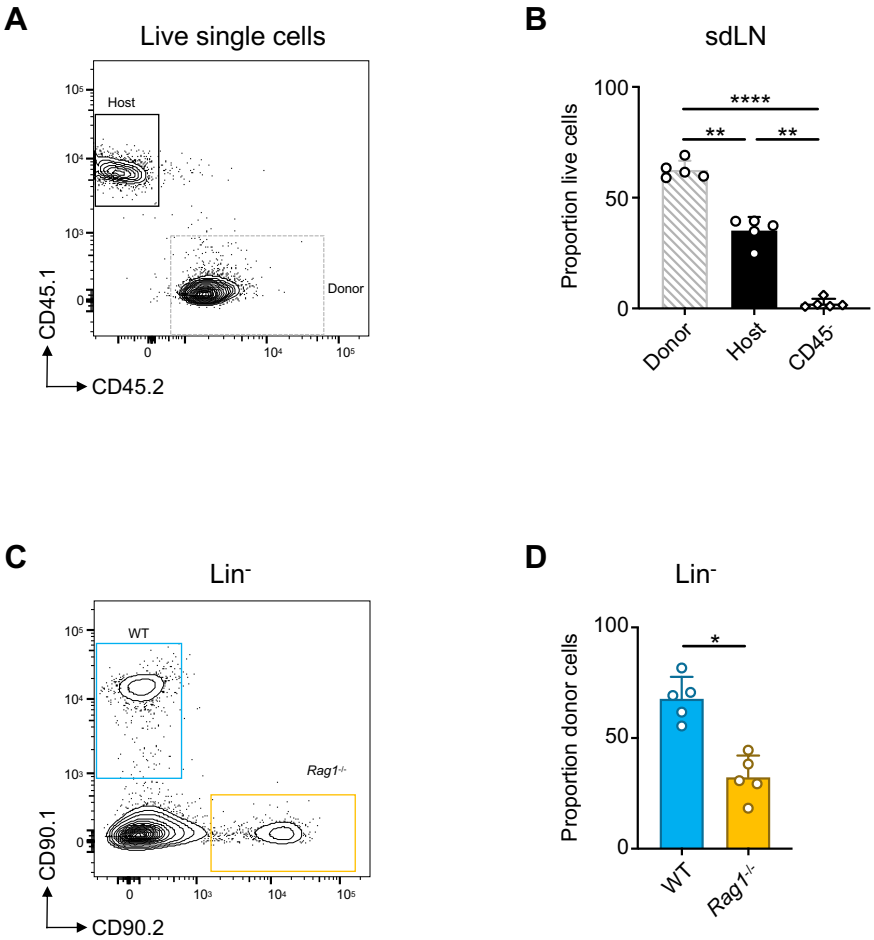
A
Live single cells
Host
Donor
CD45.1
CD45.2
B
sdLN
Proportion live cells
100
50
0
****
**
**
Donor
Host
CD45-
C
Lin-
WT
Rag1-/-
CD90.1
CD90.2
D
Lin-
Proportion donor cells
100
50
0
*
WT
Rag1-/-

Figure S5

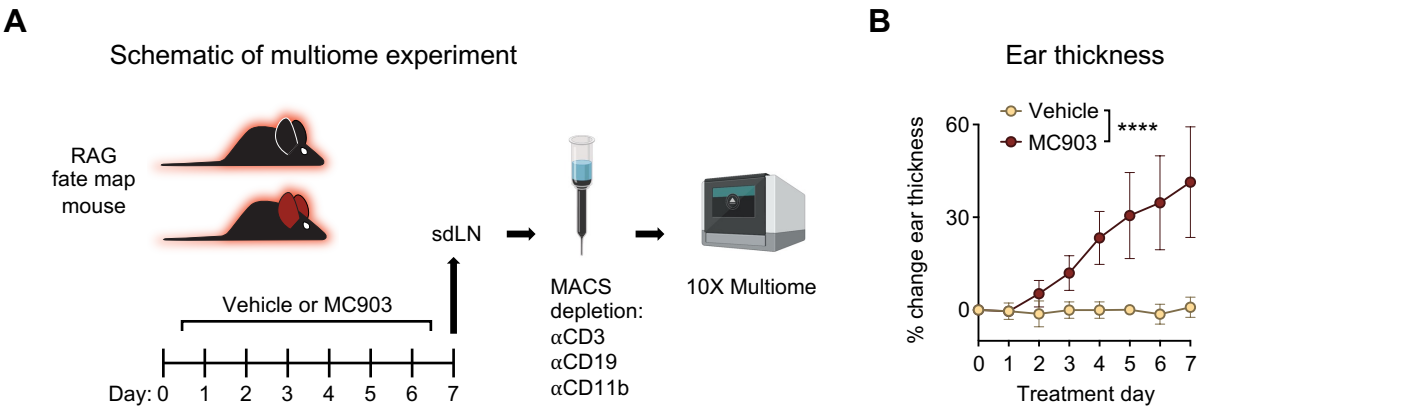
A
Schematic of multiome experiment
RAG
fate map
mouse
sdLN
Vehicle or MC903
Day: 0 1 2 3 4 5 6 7
MACS
depletion:
αCD3
αCD19
αCD11b
10X Multiome
B
Ear thickness
Vehicle
MC903
****
% change ear thickness
60
30
0
0 1 2 3 4 5 6 7
Treatment day

Figure S6

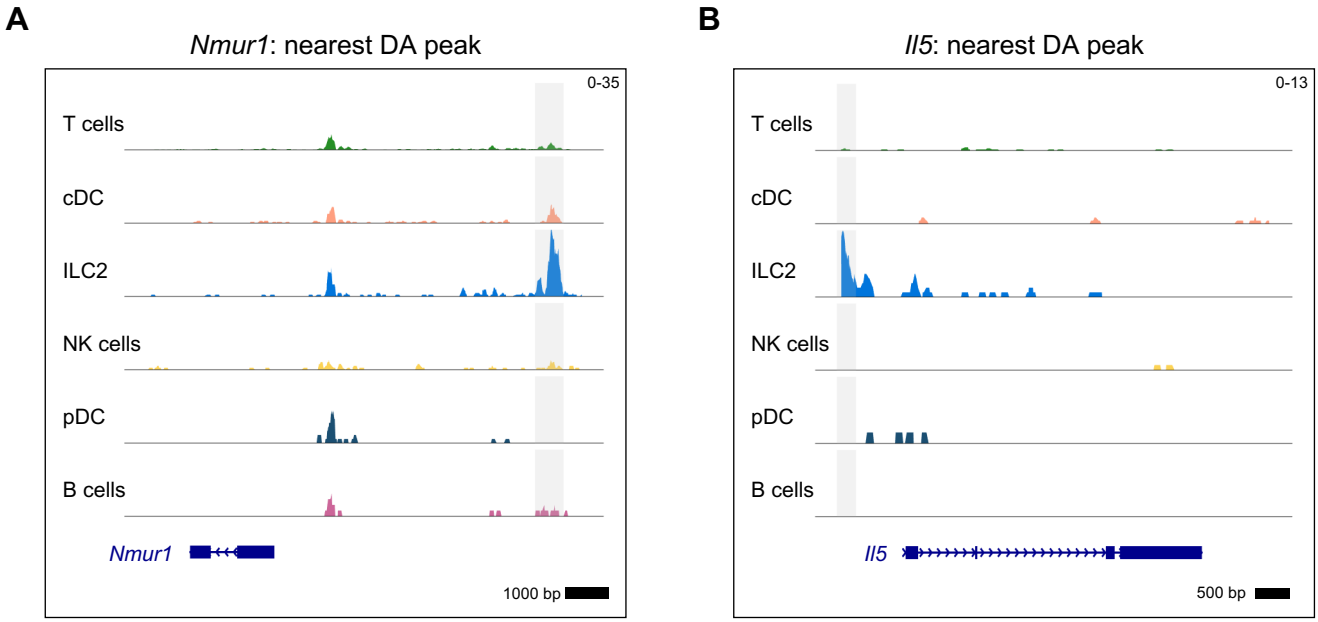
A
Nmur1: nearest DA peak
0-35
T cells
cDC
ILC2
NK cells
pDC
B cells
Nmur1
1000 bp
B
Il5: nearest DA peak
0-13
T cells
cDC
ILC2
NK cells
pDC
B cells
Il5
500 bp

Figure S7

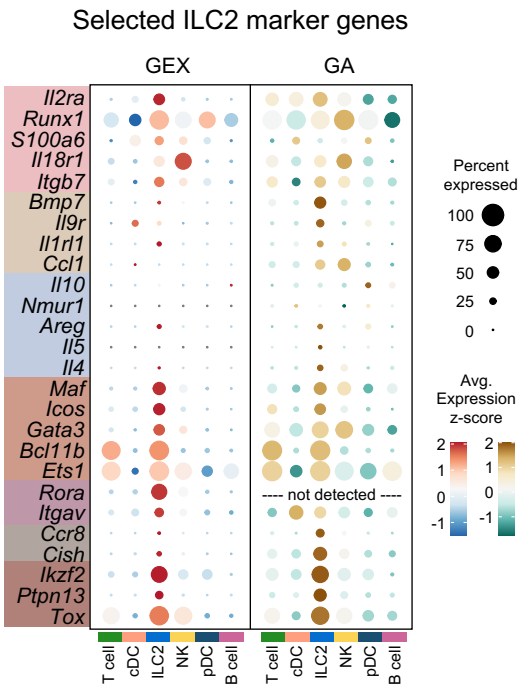
Selected ILC2 marker genes
GEX
GA
Il2ra
Runx1
S100a6
Il18r1
Itgb7
Bmp7
Il9r
Il1rl1
Ccl1
Il10
Nmur1
Areg
Il5
Il4
Maf
Icos
Gata3
Bcl11b
Ets1
Rora
Itgav
Ccr8
Cish
Ikzf2
Ptpn13
Tox
---- not detected ----
T cell
cDC
ILC2
NK
pDC
B cell
Percent expressed
100
75
50
25
0
Avg. Expression z-score
2
1
0
-1

Figure S8

A

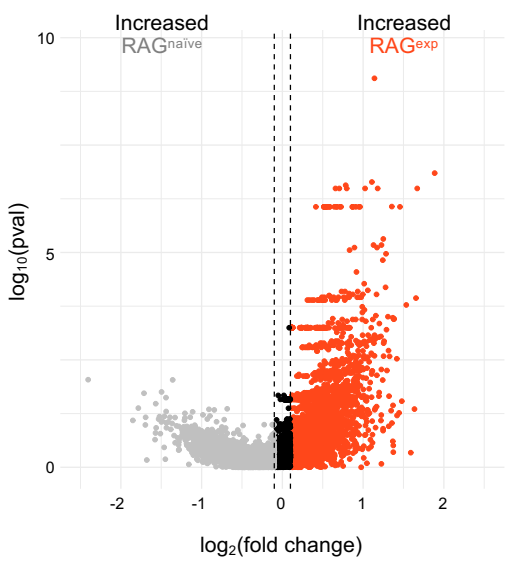

B

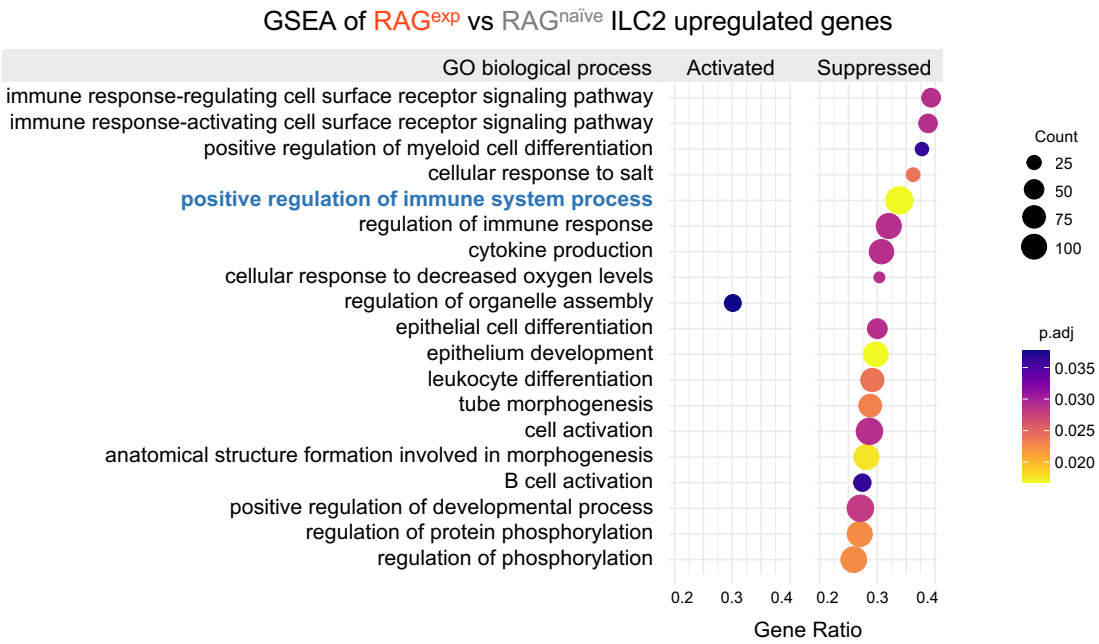

C

GO BP: **positive regulation of immune system process**

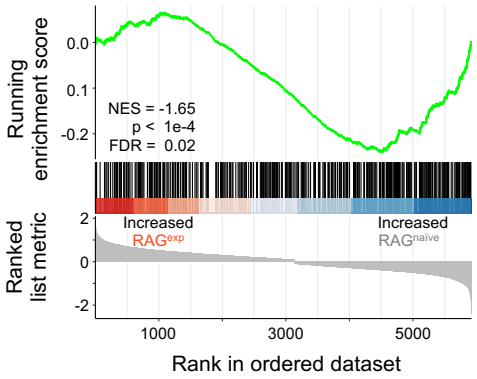

Figure S9

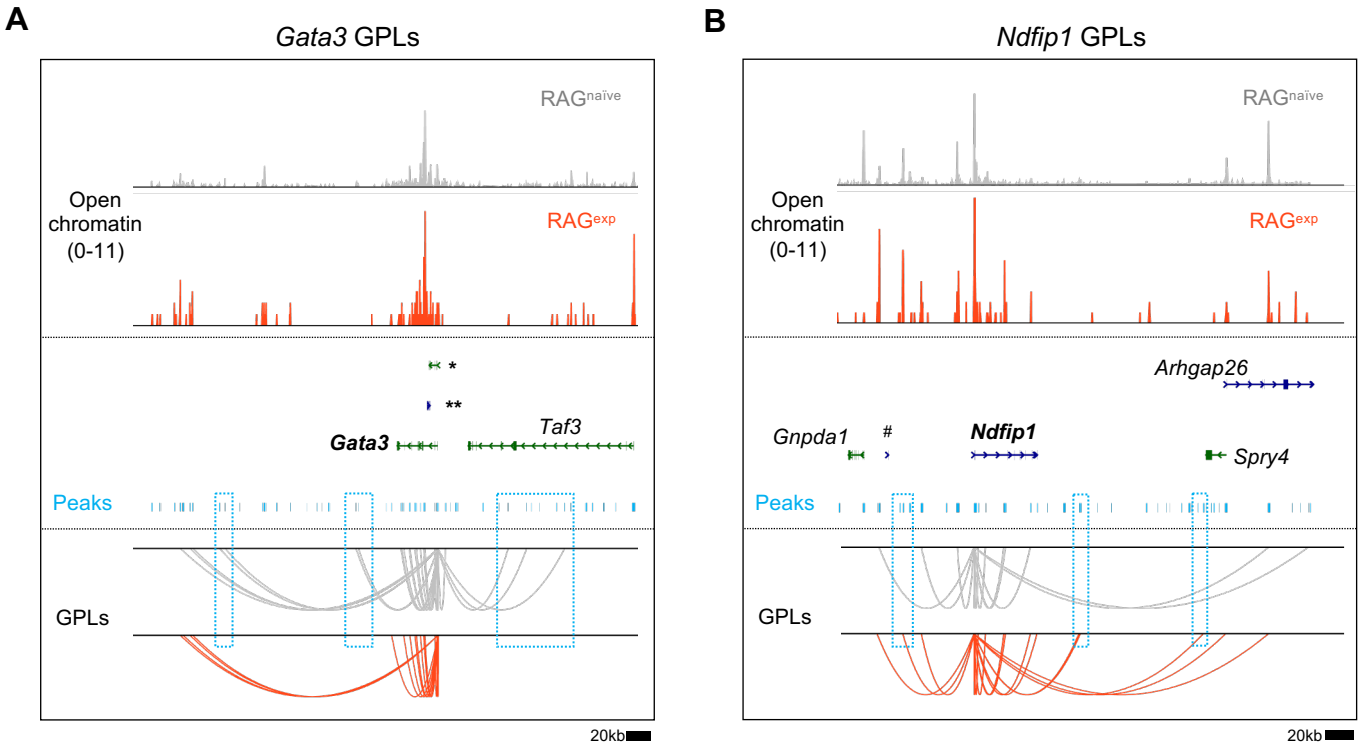
A
Gata3 GPLs
RAGnaïve
Open chromatin (0-11)
RAGexp
*
**
Gata3
Taf3
Peaks
GPLs
20kb
B
Ndfip1 GPLs
RAGnaïve
Open chromatin (0-11)
RAGexp
Arhgap26
Gnpda1
#
Ndfip1
Spry4
Peaks
GPLs
20kb

Figure S10

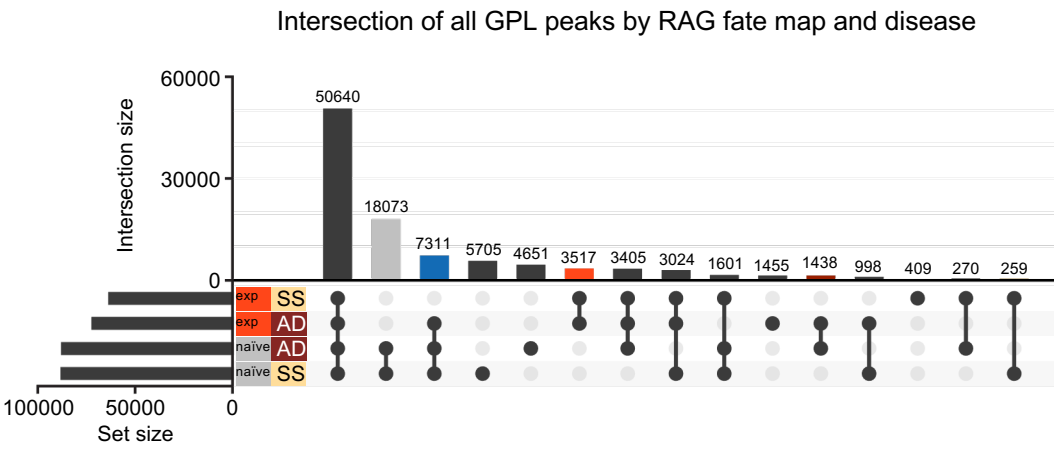
Intersection of all GPL peaks by RAG fate map and disease
Intersection size
60000
30000
0
50640
18073
7311
5705
4651
3517
3405
3024
1601
1455
1438
998
409
270
259
exp SS
exp AD
naïve AD
naïve SS
100000
50000
0
Set size